C.E.D. Riboldi
An Optimal Approach to the Preliminary Design of Small Hybrid-Electric Aircraft
Aerospace Science and Technology, Vol. 81, 2018, p. 14-31
doi:10.1016/j.ast.2018.07.042

An Optimal Approach to the Preliminary Design of Small Hybrid-Electric Aircraft

Carlo E.D. Riboldi*

[a]*Department of Aerospace Science and Technology, Politecnico di Milano, Milano, Via La Masa 34, 20156 Italy*

Abstract

Hybrid-electric propulsion is an interesting alternative for the light aviation market, carrying the advantages of electric propulsion in terms of lower noise and pollutive emissions in terminal maneuvers, while not renouncing to the flight performance – especially range – typical to conventional propulsion, based on hydrocarbon fuel. Some difficulty in the spreading of this new technology in light aviation may be ascribed to the lack of consolidated techniques to preliminary design hybrid-electric aircraft, complicating the negotiation of specifications and making design choices difficult. This is also the effect of a notable increase in the number of design variables needed to describe the hybrid-electric power-train, which include characteristics of both its thermal and electric parts, with respect to conventionally powered aircraft. The present paper presents a methodology to efficiently cope with this design problem. The procedure is based on an optimal approach where take-off weight is minimized, and constraints are included to assure meeting the mission performance requirements while not exceeding any technological limit. The paper recalls at first some simple mathematical models, allowing to translate flight performance requirements into constraints on the power-train. Then the proposed optimal design approach is thoroughly presented at a theoretical level. Finally, an example design of a hybrid-electric motor-glider is shown, where the optimal design tool is used both to find a baseline solution and to investigate the sensitivity of that design point with respect to constraints due to performance requirements and technological specifications.

Keywords:

hybrid-electric, aircraft design, preliminary sizing, optimal approach

Nomenclature

$\boldsymbol{H}$	Set of constraints
A,B	Take-off vs. empty weight regression coefficients

*Corresponding author, *Tel.:* +39-02-2399-8609; *Fax:* +39-02-2399-8334.
Email address: carlo.riboldi@polimi.it (Carlo E.D. Riboldi)

AR	Aspect ratio
C,D	Weight vs. power of electric motor regression coefficients
$C_{D,0}$	Parasite drag coefficient in parabolic polar
C_L	Lift coefficient
E_{bat}	Energy level of battery
E_f	Energy level of fuel
E_0	Total energy level
EM	Electric motor
GA	General aviation
H	Constraint identifier in set $\boldsymbol{H}$
ICE	Internal combustion engine
J	Merit function for optimization
K	Induced drag coefficient in parabolic polar
L	Length of take-off run
P_a	Available power
P_f	Required power due to wheel friction
$P_{\text{ICE},n}$	Nominal power of ICE
$P_{\text{ICE}_{\text{min},DB}}$	Minimum power of ICE in the database of real data
$P_{m,n}$	Nominal power of EM
P_r	Required power due to aerodynamics
P_{rec}	Battery charging power
S	Area of reference surface
T	Time duration
UL	Ultra-light

V	Airspeed
V_v	Rate of climb
W_{bat}	Battery weight
W_e	Empty weight
W_f	Fuel weight (initial)
W_{ICE}	Weight of ICE group
$W_{\text{ICE}_{\text{min},DB}}$	Minimum weight of ICE group in the database of real data
W_m	Weight of EM group
W_{pl}	Payload weight
$\boldsymbol{q}$	Set of optimization parameters
$\bar{\boldsymbol{q}}$	Set of optimization parameters accounting for discretization in time
$\boldsymbol{s}$	Set of time-discretized values of the throttle parameter function σ^*
e_{bat}	Specific energy of battery
e_f	Specific energy of hydrocarbon fuel
f	Shape function
g	Gravity
h	Altitude
k	Time index
p_{bat}	Specific power of battery
t	Time
β	Percentage limit on regression coefficients
η_C	Efficiency of the battery charging process
η_{ICE}	Conversion efficiency of ICE
$\eta_{\text{ICE},n}$	Nominal conversion efficiency of ICE

η_m	Conversion efficiency of EM
η_P	Propulsive efficiency of the propeller
μ	Friction coefficient
ν	Percentage limit defining minimum battery residual energy
ρ	Density of air
σ	Generic throttle setting
ξ	Percentage limit defining residual energy
σ_{ICE}	Throttle setting of ICE
σ_m	Throttle setting of EM
$(\cdot)_{\text{final}}$	Related to the end of a phase of the flight
$(\cdot)_{\text{initial}}$	Related to the beginning of a phase of the flight
$(\cdot)_{\text{lower}}$	Lower limit
$(\cdot)_{\text{ref}}$	Reference value
$(\cdot)_{\text{upper}}$	Upper limit
$(\cdot)^{\text{climb}}$	Related to climb phase
$(\cdot)^{\text{cruise}}$	Related to cruise phase
$(\cdot)^{\text{loiter}}$	Related to loiter phase
$(\cdot)^{\text{to}}$	Related to take-off phase
$\dot{(\cdot)}$	Time derivative
$(\cdot)^*$	Function of time
$\bar{(\cdot)}$	Discretized in time

1. Introduction

In recent times, electric propulsion for aircraft has been in the focus of designers and manufacturers of ultra-light (UL) and light general aviation (GA) aircraft, who see in this kind of power-train a possible way to decrease noise and chemical pollution. Considering the specific case of internal combustion engines (ICE), by far the most popular propulsion system in this category, the engine is often identified as the primary source of the overall noise footprint on ground, as well as a major responsible for limited cabin comfort [1, 2, 3]. Furthermore, being bound to combustion as an energy conversion method, ICEs are intrinsically less energy-efficient than electric motors (EM), and they invariably release chemicals in the atmosphere as side products of the conversion process, whereas electric motors perform an emission-free conversion. These advantages make the use of EMs really attractive when public acceptance is at a premium [4], as for the case of small private and sport aircraft, typically operating from smaller airports located in crowded areas, and often raising noise and chemical pollution issues [5].

The chance of electric motors to be adopted as the main power-plant for innovative light aircraft designs is currently limited, due to both a lack of confidence of the potential customers in this radically new technological application, and more substantially to the technological limit of nowadays batteries [6, 7, 8, 9, 10]. The latter feature low and penalizing specific energy and power figures, which in turn translate into a very high weight and volume toll on the aircraft, often impacting on the range and endurance of purely electric designs. A study in the field of the design of all-electric light aviation aircraft has been carried out [11], showing a systematic methodology for the preliminary sizing of these aircraft at the current level of technology. Among other results, it was highlighted that the typical mission profiles of electric aircraft can be based only on short cruises and loiter times, typically necessary to increase time in flight allowing for multiple landing circuits, thus in practice relegating these models to training missions typically performed not far from the field. It is shown that, while some examples of purely electric aircraft indeed exist, the substantial limits of this technology are currently hampering its wide adoption in aeronautics, as testified also by the limited literature on the matter. Other studies often concentrate on specific missions, where purely-electric propulsion is thought to become viable and advantageous with respect to existing ICE-propelled systems in the near future [12].

In this scenario, the hybrid-electric alternative seems to put together the advantages of ICEs and EMs, allowing to increase efficiency and reduce emissions without renouncing to a good flight performance. The idea of hybrid-electric propulsion has been developed well into the production stage in the automotive sector [13, 14]. Concerning the adoption of hybrid-electric propulsion in aeronautics, a substantial analysis of the performance and an identification of the design indices allowing to characterize and compare hybrid-electric aircraft over different weight categories has been carried out to a good extent in some recent works [15, 16, 17, 18], encompassing some diverse hybrid concepts and configurations not limited to ICE for the fuel-

burning component, and extending to distributed propulsion. Some example designs based on hybrid-electric propulsion systems have been described for instance in [19], dealing with a re-engined version of an existing UL. Notwithstanding the appreciable knowledge-base, hybrid-electric aircraft have been developed only rarely beyond the conceptual design phase [20, 21].

The reasons for that can be found on one side in the high risk perceived by the stakeholders when experimenting with the application of a new technology in the aviation field, similarly to the case of electric aircraft [11]. Furthermore, a comprehensive practical approach to the sizing of a hybrid-electric aircraft from an assigned set of requirements has not been envisaged yet. A limited effort in this sense has been documented for instance in [22], yet in that work the sizing of the hybrid-electric power-train has been constrained by stringent hypotheses.

The present paper moves farther in this research area, and outlines a possible new general methodology to face the preliminary sizing of a hybrid-electric aircraft, considering the UL or lighter GA category as a field for testing. The proposed design procedure is based on an optimal approach which had not been investigated in previous works, aimed to the direct solution of the sizing problem, where a suitable optimization method is deployed to target the components of take-off weight through a suitable measure of merit. Multiple constraints, coming from the mission analysis and certification barriers as well, are put in mathematical terms. Similarly, the power and weight characteristics and limits of the hybrid power-plant, composed of a single ICE and a single EM in this study, will be formulated as constraints in the optimization process. In order to make this study more readily usable, a stress is put on using most of the existing methodologies developed for conventional propulsion [23, 24] and more recently emended to cope with the peculiarities of purely electric propulsion [11]. The design approach starts from an initial guess identified in terms of power loading and wing loading, such to comply with some mission and certification requirements. It will be shown how to set up an optimal problem where the weights summing up to the take-off weight can be configured as optimization variables. In particular, the selected weights of the ICE and EM will be bound to the corresponding nominal power figures, thus implying a certain power installed. Furthermore, in order to find a proper way to set the power mix coping with the requirements of each phase of the flight, and accounting for the change of fuel weight over time, the selection of a throttle setting for the two power sources, considered as a function of time, will be demanded to the optimizer. The overall process is therefore configured as a comprehensive optimal approach, where weight components, power and power management settings are adjusted in a coordinated fashion to guarantee the lowest design weight possible while satisfying flight performance requirements.

An application of the presented methodology will be demonstrated on a realistic sizing problem, following a critical approach to the analysis of the results.

The primary application of the present paper is limited to the light aviation category – based on the

relatively low power and weights considered, as well as the modest mission requirements –, which represents an easier potential market thanks to the less stringent certification rules. Furthermore, more technological data is available in this sector, making the adoption of futuristic or highly uncertain assumptions less necessary. Moreover, the power and energy needs of lighter aircraft can be more easily coped with by considering just one ICE and EM at most, in turn allowing to simplify the analysis neglecting issues typical to distributed propulsion or less usual hybrid-electric power-plant configurations. With these considerations, it is reasonable to expect that a prototype could be more readily designed following the methodology presented herein in the light aviation category. Nonetheless, this procedure can be easily modified to account for requirements typical to more aircraft categories, hence potentially greatly enlarging the scope and applicability of the present work.

2. Hybrid-electric aircraft characterization and sizing concepts

2.1. Design take-off weight and its components

The preliminary sizing procedure of an aircraft is centered on the determination of the weight components appearing in the breakdown of its design take-off weight [23, 24]. The first major component of this procedure is the relationship between the empty weight W_e and the design take-off weight W_{to}. This relationship usually comes from the analysis of previously completed designs in the same aircraft configuration and mission category of the new design of interest [23, 24]. As long as the intended aircraft is not to perform an atypical mission, employ totally new technologies, or display a very unusual configuration, it is typically possible to find a sufficient number of aircraft already designed in the corresponding category, allowing to setup a data regression between W_e and W_{to}. For the case of electric aircraft, which are still today not widespread and all in the lightest weight category, this analysis has been performed, yielding a relationship in the form proposed by Roskam [23],

$$\log(W_{\text{to}}) = A + B\log(W_e), \tag{1}$$

where the coefficients A and B are computed from the regression of data. Figure 1 shows the data and regression line for a group of electric aircraft in the UL or GA category [11].

It should be remarked that the empty weight W_e is basically the weight of the aircraft structure and on-board systems without a function in the power-train. The weights of the power-train, energy storage elements - i.e. for instance batteries and fuel for the type of hybrid-electric aircraft of interest here - and of course of the payload are accounted for separately. For the sake of clarity, note that in this paper all weights are considered as forces, hence they are measured in Newtons (N) or multiples. When the corresponding masses are considered in plots or tables, they are properly referred to using the ratio W/g, where g is gravitational acceleration. This expression for mass stems from the usual relationship between mass and weight force. Masses are expressed in kilograms (kg).

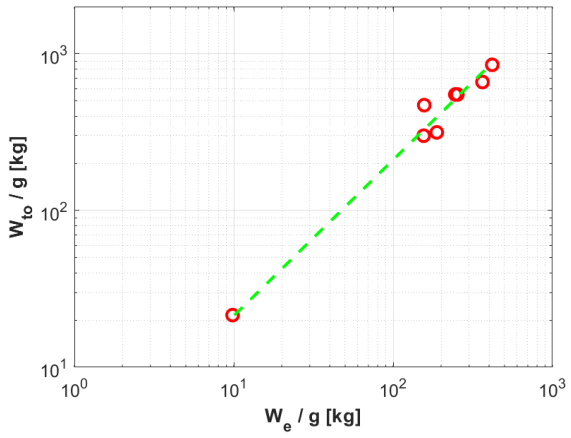

Figure 1: Take-off weight W_{to} vs. empty weight W_e for light purely-electric aircraft. Red circles: real data. Green dashed line: regression.

When the proposed design is placed in a new aircraft category – like for small hybrid-electric aircraft – or the share of innovation is very high with respect to existing exemplars, a similar relationship can still be used, but some more considerations are needed. It can be observed that in order to ensure a sufficient number of aircraft for a meaningful statistical approach yielding the coefficients of Eq. 1, it may be necessary to include designs responding only to a part of the required criteria of commonality, i.e. typically mission category, configuration or technological level. Aircraft with a similar mission but from older times will be discarded in the database processing phase, privileging more recent ones, which usually involve a higher share of new technology. In any case, the result of the data regression will be more loosely descriptive of the actual relationship between weights for the new aircraft. This effect can be accounted for in two ways *a posteriori*. Firstly, Eq. 1 can be used in statistical terms, defining acceptable bounds for coefficients A and B, thus relaxing the adherence of the final design solution to a mathematically exact relationship expressed by Eq. 1. This is particularly practical in an optimal solution approach, as will be better shown in a later stage of this work. Secondarily, a sensitivity analysis may be performed on the design solution for perturbed values of coefficients A and B in Eq. 1. This analysis may show a little effect of one or both parameters on the final results, highlighting whether the adopted level of accuracy on the regression parameters is acceptable or not.

The second component in the weight sizing procedure is the definition of the breakdown of the design take-off weight, and its characterization through the analysis of the mission profile [23, 24]. For conventional ICE- or jet-propelled aircraft, the well proven method of the fuel fractions can be profitably applied to obtain a second relationship between W_e and W_{to} from the breakdown of design take-off weight. Flanking Eq. 1 with this new relationship allows to setup a non-linear system in W_e and W_{to} which can be easily solved. From W_{to} and the fuel fractions it is possible to obtain all weight components in the breakdown of the design

take-off weight. For purely electric aircraft with a traditional configuration, a more elaborated method based on the use of the sizing matrix plot (SMP) has been thoroughly described in [11], dealing with the fact that electrically propelled aircraft do not lose weight during the flight, thus hampering the very definition of fuel fractions. Similarly, in order to treat the hybrid-electric case of interest here, based on an internal combustion engine and an electric motor, it is necessary to introduce a suitable weight breakdown, where all components will be subsequently characterized. The proposed definition of the design take-off weight for a hybrid-electric aircraft is presented in Eq. 2

$$W_{\text{to}} = W_{\text{ICE}} + W_f + W_m + W_{\text{bat}} + W_e + W_{\text{pl}}, \tag{2}$$

where W_{ICE} is the weight of the internal combustion engine group, W_f the weight of stored hydrocarbon fuel, W_m the weight of the electric motor group, W_{bat} the weight of batteries and W_{pl} that of payload. The internal combustion engine group is composed of the ICE itself, and all mechanisms necessary for allowing the transfer of mechanical power to the propeller and to the battery, including a gearbox and an electrical generator. On the other hand, the electric motor group contains the EM and the related gearbox necessary to transfer power to the propeller. It should be observed that at the level of Eq. 2 the number of ICEs or EMs intended to be fit in the design is not an issue.

In order to solve the system composed of Eq. 1 and 2, it would be necessary to obtain from the latter equation an expression in terms of W_e and W_{to}. Similarly to the case of purely electric aircraft, the electric component of the power-train makes it impossible to adopt fuel fractions for the task. An alternative method similar to the one suggested in [11] for purely electric aircraft is based in a first stage on the analysis of the mission profile, together with constraints coming from standard rules, through the sizing matrix plot (SMP) [24]. This allows to select some parameters which are kept fixed for the rest of preliminary design, and makes possible to explicitly write the expressions pertaining to flight performance in all phases of the flight profile, thus leading to a procedure for closing the system in W_{to} and W_e. In the present work, such expressions and the proposed way to exploit them will be shown in dedicated sections, after introducing the model of a hybrid-electric power-train.

Concerning the other weight components in Eq. 2, some of them feature a relationship with power or energy figures. These relationships come from the very constitution of these components, and can be characterized by means of statistical analyses on similarly manufactured items. Such relationships are assumed here for batteries, the ICE group and the EM group, as explained in the following.

Batteries can store energy and provide power based on their mass. The energy density e_{bat} and power density p_{bat} are intrinsic characteristics of battery packs, which can be used to define the maximum stored energy and the maximum energy flow for these components, respectively as $E_{\text{bat}}^{\max} = \frac{W_{\text{bat}} e_{\text{bat}}}{g}$ and $\dot{E}_{\text{bat}}^{\max} = \frac{W_{\text{bat}} p_{\text{bat}}}{g}$, where g is gravity acceleration.

An energy quota can be defined also for the hydrocarbon fuel stored on board. Passing from fuel weight to fuel energy can be accomplished through an expression formally similar to the one just introduced for batteries, yielding $E_f = \frac{W_f e_f}{g}$.

Due to the fact that hybrid-electric aircraft already manufactured are very few, and usually largely suboptimal, partially re-engined exemplars of existing conventional aircraft, available data is not sufficient to setup an acceptable statistical analysis. For this reason, a family of engines finding application in the parallel field of marine propulsion, but with an acceptable level of mission commonality with respect to the ICE to be included in the design of an aircraft, may be selected to obtain the necessary weight and power data [22, 25].

Two relevant points of commonality exist between the selected family of ICEs and the type of aircraft engine necessary for the intended scope. Firstly, anticipating some of the results of this study, it can be shown *a posteriori* that the optimal working condition of the ICE on board the considered hybrid-electric aircraft category considered here, looking at the most prolonged phases of the flight, is an almost constant power at a throttle setting which does not cover the total flight power requirement. Limited power – compared to typical aeronautical needs – and a constant operative regime constitute the design scenario of the considered family of engines, which are not studied to deliver a high peak performance, but are instead lightweight engines conceived to work at an almost constant output [25]. Secondarily, weight data for the marine engines considered here include a gearbox and a battery recharging device, which in turn make the determination of the weight of the ICE group, defined above as a whole, sufficiently accurate without the need to consider the weight of these components separately. The latter could be done in a future work on the topic, by extrapolating more precise data for all components of a real hybrid aircraft currently not available, but it is not a crucial point for the design procedure presented herein, which can be easily amended in this sense if needed by considering more weight components separately in Eq. 2 instead of wrapping them together.

A statistical regression of power and weight data for the selected family of ICE engines can be satisfactorily performed based on a logarithmic shape function [22], yielding

$$\begin{aligned} &\text{if}\,(P_{\text{ICE},n}) \geq P_{\text{ICE}_{\text{min},DB}} : W_{\text{ICE}} = \log(P_{\text{ICE}}) \\ &\text{if}\,(P_{\text{ICE},n}) < P_{\text{ICE}_{\text{min},DB}} : W_{\text{ICE}} = \left(\frac{P_{\text{ICE},n}}{P_{\text{ICE}_{\text{min},DB}}}\right) W_{\text{ICE}_{\text{min},DB}} \end{aligned}, \tag{3}$$

where a linear branch has been added below the minimum database entry $P_{\text{ICE}_{\text{min},DB}}$ for the nominal power of the ICE $P_{\text{ICE},n}$, to cover the lowest portion of the power domain [22].

Concerning the EM group, a sufficiently accurate regression based on the data of existing electric aircraft comes in the form [11]

$$W_m = C + DP_{m,n}, \tag{4}$$

where C and D are assigned coefficients and $P_{m,n}$ is the nominal power of the electric motor. It should be remarked that the regression is different from the one reported in previous works by the author [11, 22], as

this appears to be more physically suited, better embracing also a slightly augmented array of experimental data.

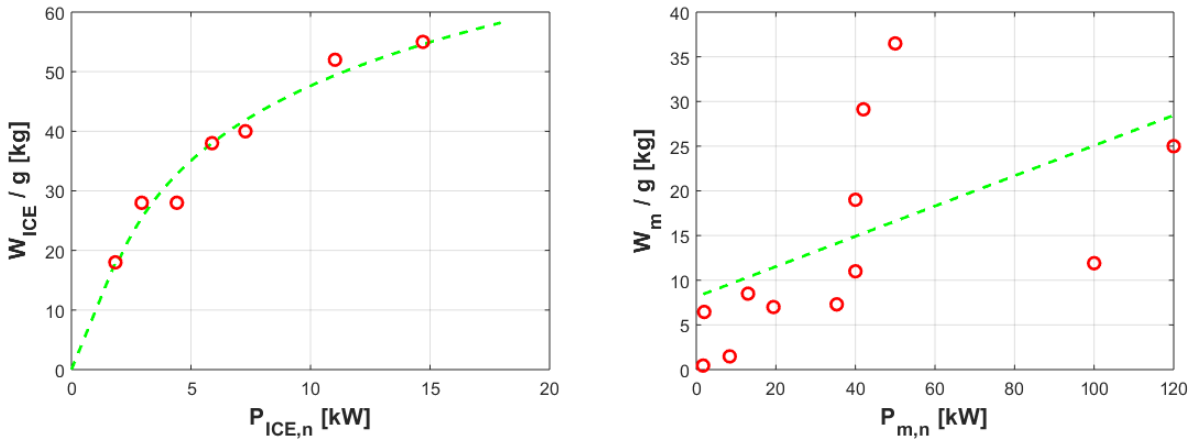

(a) (b)

Figure 2: Weight vs. power data for ICE (left) and EM (right) propulsive groups. Red circles: real data. Green dashed line: regression.

Figure 2 shows the data regression lines for a series of ICE and EM groups, to the left and right respectively.

2.2. Hybrid-electric power-train model for small aircraft

Before introducing the analysis of the sizing problem, it is necessary to derive an analytic model of the power-plant. Figure 3 shows the energy flowchart of the proposed power-train.

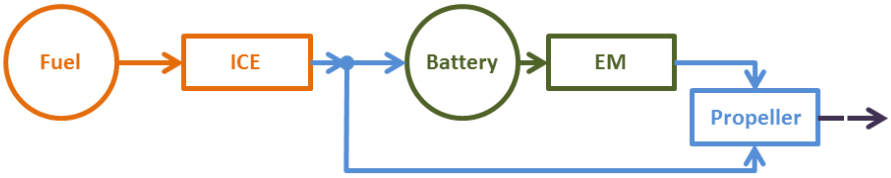

Figure 3: Energy flowchart for the considered power-train. Amber connectors: fuel flow. Blue connectors: mechanical power flow. Green connectors: electric power flow. Purple connectors: output power flow.

From left to right, it is possible to find:

- the hydrocarbon fuel storage for the ICE, associated to the design weight W_f and to the energy flow $\frac{\dot{W}_f e_f}{g}$, wherein the fuel mass flow $\frac{\dot{W}_f}{g}$ is multiplied by the fuel energy density e_f
- the ICE unit, which produces a power output $P_{\text{ICE}} = \sigma_{\text{ICE}} P_{\text{ICE},n}$, where $P_{\text{ICE},n}$ is the nominal power value of the ICE, and σ_{ICE} represents the throttle setting and varies between 0 and 1

- a splitting node where the mechanical power P_{ICE} produced by the ICE is divided in two components, namely a battery recharge component and a propulsive component
- following the electric propulsion branch on top of the scheme, the recharge power component P_{rec} feeds the battery through a generator, associated to a conversion process and a related recharge efficiency η_C, and the battery pack is associated to a weight W_{bat} and a positive energy level below $E_{\mathrm{bat}}^{\mathrm{max}} = \frac{W_{\mathrm{bat}} e_{\mathrm{bat}}}{g}$, as mentioned previously
- the battery pack is followed along the top branch of the scheme by the group of the electric motor, associated to a weight W_m and an output power $P_m = \sigma_m P_{m,n}$, where, similarly to the case of the ICE, σ_m represents a throttle setting between 0 and 1, whereas $P_{m,n}$ is the nominal power of the electric motor
- a propulsive conversion block, where the available mechanical power flows from the ICE and EM are mixed and converted into power available for the flight – typically by means of a propeller – with an associated conversion efficiency η_P.

The adopted hybrid-electric configuration can be classified as a series-parallel [17], in the sense that the mechanical power is used for recharging the batteries, but it also contributes directly to propulsion.

The energy flowchart in Fig. 3 can be promptly used to derive a series of balance relationships which will contribute substantially to the analytic setup of the sizing problem, translating flight performance requirements typical to each phase of the design mission into the corresponding required characteristics of the power-train components. These will be illustrated in the following section.

3. Performance models for mission analysis

In order to translate the desired mission performance into weight requirements it is necessary to deploy simple flight mechanics models, thus deriving analytic relationships between power, energy and weight figures, and flight performance. The flight profile of a light aircraft for sport or tourism can be imagined composed of five phases, namely take-off, climb, cruise, loiter and descent/landing [24]. In this study we concentrate on the first four, adding a safety margin on the results of the design to account for the last phase *a posteriori*, as it usually implies very little energy expenditure and low power required.

3.1. Take-off phase

The requirement on the take-off phase is usually specified as a take-off run length L^{to}, to be met at the design take-off weight W_{to} and at a certain elevation of the field, characterized by an assigned ρ^{to}. An

expression for L_{to} can be obtained starting from a power balance equation, yielding

$$\frac{W_{\text{to}} V \dot{V}}{g} = P_a^{\text{to}} - P_r^{\text{to}} - P_f, \tag{5}$$

where V is airspeed, $\dot{V}$ is the linear acceleration along the run, P_a^{to} is the available propulsive power, P_r^{to} is the power required due to aerodynamics and P_f the power required due wheel to friction. Due to the very low duration of this flight phase, the weight of the aircraft can be safely considered constant and equal to W_{to} for computations where the weight of the aircraft is involved. The change in weight can be computed and accounted for *a posteriori*.

The required power P_r^{to} due to aerodynamics will be a function of airspeed, which increases during the run up to the take-off speed V^{to}. The latter can be computed based on the value of the lift coefficient of the aircraft during the take-off run, which is constant if the rotation phase is excluded from the take-off maneuver – as a matter of fact, rotation does not add significantly to the take-off run especially for smaller aircraft, so this is not a heavy assumption. The value of the lift coefficient C_L^{to} is not necessarily the stall value but typically smaller for safety, yet it may account for a lift curve corresponding to deployed flaps and/or slats, which needs to be characterized through preliminary analysis. In analytic terms, P_r^{to} in Eq. 5 can be written as a function of V as [26]

$$P_r^{\text{to}} = \frac{1}{2}\rho^{\text{to}} V^3 S \left(C_{D,0}^{\text{to}} + K^{\text{to}} C_L^{\text{to}^2} \right), \tag{6}$$

where coefficients $C_{D,0}^{\text{to}}$, K^{to} and C_L^{to} are typical to the parabolic polar of the aircraft in take-off configuration, and S is the area of the wing reference surface [24].

The power required due to wheel friction P_f in Eq. 5 can be written as a function of a friction coefficient μ dictated by the tire-surface coupling, and proportional to the reaction force normal to the runway, itself a difference between the weight and the current lift value, function of the airspeed. This yields

$$P_f = \mu \left(W_{\text{to}} - \frac{1}{2}\rho^{\text{to}} V^2 S C_L^{\text{to}} \right) V. \tag{7}$$

By substituting Eq. 6 and 7 into Eq. 5, recalling that $\dot{V} = \frac{\mathrm{d}V}{\mathrm{d}t}$ and $\mathrm{d}t = \frac{\mathrm{d}s}{V}$ it is possible to isolate the run differential distance $\mathrm{d}s$, and integration yields

$$L^{\text{to}} = \int_0^{V^{\text{to}}} \frac{\frac{W_{\text{to}}}{g} V^2}{P_a^{\text{to}} - \left(\frac{1}{2}\rho^{\text{to}} V^3 S \left(C_{D,0}^{\text{to}} + K^{\text{to}} C_L^{\text{to}^2} - \mu C_L^{\text{to}} \right) + \mu W_{\text{to}} V \right)} \mathrm{d}V. \tag{8}$$

The value of available propulsive power P_a^{to} is a result of the throttle settings, and can be expressed starting from the power flowchart in Fig. 3 as

$$P_a^{\text{to}} = \eta_P \left(\sigma_{\text{ICE}}^{\text{to}} P_{\text{ICE},n} + \sigma_m^{\text{to}} P_{m,n} - P_{\text{rec}}^{\text{to}} \right), \tag{9}$$

where $P_{\text{rec}}^{\text{to}}$ is the value of recharge power in take-off, i.e. the component of available ICE power destined to battery recharging, and not to propulsion.

Concerning the level of stored energy, as mentioned above the weight of the aircraft can be considered constant due to the short duration of this phase for the evaluation of Eq. 8. For better precision, the value of weight at the end of take-off can be obtained based on the computation of $W^{\mathrm{to}}\left(t_0^{\mathrm{to}}+T^{\mathrm{to}}\right)=W^{\mathrm{to}}\left(t_0^{\mathrm{to}}\right)-\frac{\sigma_{\mathrm{ICE}}P_{\mathrm{ICE},n}g}{e_f\eta_{\mathrm{ICE}}}T^{\mathrm{to}}$, where η_{ICE} represents the conversion efficiency of the ICE, t_0^{to} the initial time and $T^{\mathrm{to}}=\int_0^{V^{\mathrm{to}}}\frac{\mathrm{d}V}{\dot{V}}$ the time extension of the take-off run.

For the battery, the corresponding energy flow, considered negative when the energy level is decreasing, can be written as

$$\dot{E}_{\mathrm{bat}}^{\mathrm{to}}=\eta_C P_{\mathrm{rec}}^{\mathrm{to}}-\frac{\sigma_m^{\mathrm{to}}P_{m,n}}{\eta_m}, \tag{10}$$

where η_m represents the conversion efficiency of the electric motor.

The battery energy quota $E_{\mathrm{bat}}^{\mathrm{to}}$ for take-off can be computed integrating the expression of $\dot{E}_{\mathrm{bat}}^{\mathrm{to}}$ in Eq. 10 in time over the duration of the take-off phase. This yields

$$E_{\mathrm{bat}}^{\mathrm{to}}=\int_0^{T^{\mathrm{to}}}\dot{E}_{\mathrm{bat}}^{\mathrm{to}}\mathrm{d}t. \tag{11}$$

Finally, the total energy needed for take-off, coming from the sum of the fuel and battery energy components, can be written as

$$E_0^{\mathrm{to}}=E_f^{\mathrm{to}}+E_{\mathrm{bat}}^{\mathrm{to}}. \tag{12}$$

3.2. Climb, cruise and loiter

From the viewpoint of the power and energy computations of interest here, the three phases of climb, cruise and loiter can be treated the same way.

A general expression for the required power can be obtained for a generic phase of the flight starting from aircraft vertical equilibrium as [26]

$$P_r=V_vW+\left(\frac{1}{2}\rho SV^3C_{D,0}+K\frac{W^2}{\frac{1}{2}\rho SV}\right), \tag{13}$$

where in principle V_v, W, ρ and V are all functions of time, whereas $C_{D,0}$ and K may change according to the aircraft configuration. The most typical requirement for the climb phase comes in the form of an assigned rate of climb V_v, which translates into a climb duration when a difference between the starting and target altitudes is defined. Therefore, for this phase V_v will be assigned based on the respective requirement, whereas for cruise and loiter this parameter will be null. On consideration of the limited range of operative altitudes for light general aviation aircraft, which typically fly well below 10'000 ft for physiological limits bound to pressurization, the value of air density ρ for climb can be assigned to a reference value, intermediate between the starting and final levels of the climb. For cruise and loiter, ρ can be set to the respective intended value. Similarly, the speed value V can be assigned for each phase, and considered constant for simplicity for

the corresponding time extension. Finally, the parameters of the parabolic polar $C_{D,0}$ and K can be assigned to different values for the three phases, accounting for different flap/slats or landing gear configurations.

Recalling that the focus is here on light aircraft, it is common practice to perform constant speed and altitude cruise and loiter phases in this category, so the assumption of constant ρ and V in Eq. 13 for each of them does not constitute a heavy limitation. In case these hypotheses are not satisfied over the whole duration of these parts of the flight profile, cruise and loiter can be subdivided into shorter intervals, where such hypotheses apply more accurately. Furthermore, when deemed necessary the mission profile can be made more sophisticated by adding multiple climb, cruise and loiter phases with different specifications, without significant changes to the approach presented in this work.

It should be remarked that differently from the take-off phase previously examined, the value of weight W is here a function of time in all computations, and as such will be indicated as W^*. Being the only weight component to cause a change in the overall weight, studying the fuel weight W_f^* makes possible to monitor the evolution of W^*. Fuel weight can be computed at every time instant in a phase of the flight as

$$W_f^* = W_{f,\tau=t_0} - \int_{t_0}^{t} \frac{\sigma_{\mathrm{ICE}}^* P_{\mathrm{ICE},n} g}{e_f \eta_{\mathrm{ICE}}} \mathrm{d}\tau, \tag{14}$$

where t_0 stands for the initial time of the considered phase, t the current time instant measured from the beginning of the mission, and superscript $(\cdot)^*$ refers to a generic phase of the flight, allowing to distinguish W_f^*, which is a function of time, from the overall fuel weight W_f for the complete mission. It should be noticed that the throttle setting σ_{ICE}^* in Eq. 14 is in general an assigned function of time, whereas $P_{\mathrm{ICE},n}$ is a constant reference value.

The corresponding evolution of the fuel energy level can be tracked through

$$E_f^* = \frac{W_f^* e_f}{g}. \tag{15}$$

The overall weight of the aircraft will vary proportionally to W_f^*, as

$$W^* = W_{\tau=t_0} - W_f^*, \tag{16}$$

where, similarly to W_f^*, W^* represents a function of time for the considered phase of the flight.

In order to compute the time history of battery energy E_f^*, it is necessary to compute the recharge power P_{rec}, which can be obtained from the power flowchart in Fig. 3 hypothesizing a power balance such that $P_a^* = P_r^*$, as

$$P_{\mathrm{rec}}^* = \sigma_{\mathrm{ICE}}^* P_{\mathrm{ICE},n} + \sigma_m^* P_{m,n} - \frac{P_r^*}{\eta_P}. \tag{17}$$

Here again, the throttle settings σ_{ICE}^* and σ_m^* are functions of time, whereas P_r^* can be obtained evaluating Eq. 13 for the current value of weight W^*. From the recharge power computed in Eq. 17 it is possible to

obtain the battery energy flow $\dot{E}^*_{\text{bat}}$ with an equation formally identical to Eq. 10 for the case of take-off, yielding

$$\dot{E}^*_{\text{bat}} = \eta_C P^*_{\text{rec}} - \frac{\sigma^*_m P_{m,n}}{\eta_m}, \tag{18}$$

and similarly by integrating the flow over time like in Eq. 11 it is possible to track the energy of the battery, yielding

$$E_{\text{bat}} = E_{\text{bat},\tau=t_0} + \int_{t_0}^{t} \dot{E}^*_{\text{bat}} \mathrm{d}\tau. \tag{19}$$

Finally, the time history of the overall energy level can be obtained as

$$E^*_0 = E^*_{\text{bat}} + E^*_f. \tag{20}$$

3.3. Total design values for the mission

By applying the models recalled above for take-off and for the three phases of climb, cruise and loiter, it is possible to obtain the values of weight, energy and power needed to complete the mission. To this aim, it is necessary to preliminarily compute the time duration of the latter three phases of the mission. This can be readily done under the assumptions of constant speed, and of constant vertical speed for climb. For the climb phase,

$$T^{\text{climb}} = \frac{\Delta h}{V_v}, \tag{21}$$

where Δh is the vertical distance which the aircraft is required to cover.

For cruise and loiter the mission requirements include typically a distance to cover and a flight time respectively. Consequently, the duration of cruise can be computed as

$$T^{\text{cruise}} = \frac{R^{\text{cruise}}}{V^{\text{cruise}}}, \tag{22}$$

where the range R^{cruise} is assigned.

For loiter, the duration will be directly specified by the requirement through T^{loiter}.

Now, in computational terms the overall take-off design weight can be built up based on Eq. 2 component by component. Starting from the fuel weights pertaining to each phase of the flight, under the assumption of constant weight during the usually short take-off phase, it is possible to write

$$W_f = W_f^{\text{to}} + W_f^{\text{climb}} + W_f^{\text{cruise}} + W_f^{\text{loiter}}, \tag{23}$$

where each component on the right hand side except W_f^{to}can be obtained integrating Eq. 14 over the time length of the corresponding phase defined in Eqs. 21, 22 for climb and cruise, and assigned as a requirement for loiter.

In order to compute the weight of the batteries W_{bat} it is first necessary to compute the required battery peak power and the energy to store in the batteries. Battery energy can be computed as

$$E_{\text{bat}} = E_{\text{bat}}^{\text{to}} + E_{\text{bat}}^{\text{climb}} + E_{\text{bat}}^{\text{cruise}} + E_{\text{bat}}^{\text{loiter}}, \tag{24}$$

where each component of the total battery energy for the flight E_{bat} is obtained by integration from Eq. 19, and from Eq. 11 for take-off. The peak power of the battery can be obtained from the maximum of $\dot{E}_{\text{bat}}$ recorded over each phase of the flight – Eq. 10 and 18 – as

$$\dot{E}_{\text{bat}}^{\text{max}} = \max\left\{\dot{E}_{\text{bat}}^{\text{to}}, \dot{E}_{\text{bat}}^{\text{climb}}, \dot{E}_{\text{bat}}^{\text{cruise}}, \dot{E}_{\text{bat}}^{\text{loiter}}\right\}, \tag{25}$$

where it should be noted that $\dot{E}_{\text{bat}}^{\text{climb}}$, $\dot{E}_{\text{bat}}^{\text{cruise}}$ and $\dot{E}_{\text{bat}}^{\text{loiter}}$ are functions of time.

Based on Eqs. 24 and 25 it is possible to define the weight of the battery based on the most requiring request as

$$W_{\text{bat}} = \max\left\{\frac{E_{\text{bat}} g}{e_{\text{bat}}}, \frac{\dot{E}_{\text{bat}}^{\text{max}} g}{p_{\text{bat}}}\right\}. \tag{26}$$

Finally, in order to compute the weight of the ICE and EM groups it is sufficient to know the nominal power $P_{\text{ICE},n}$ and $P_{m,n}$. These should be set to satisfy the mission requirements and providing a power balance at any time during the flight. More in depth, considering the instantaneous power available through the ICE and EM, it is clear that this power will need to be modulated over time to satisfy power balance. To this aim, as $P_{\text{ICE},n}$ and $P_{m,n}$ are two constant parameters, it is necessary to assign the throttle settings as time functions, in order to allow scaling power as required for different phases of the flight. Furthermore, in those phases where weight is changing, i.e. by hypothesis during climb, cruise and loiter, this will allow to further adjust power to guarantee equilibrium.

Putting $P_{\text{ICE},n}$ and $P_{m,n}$ into Eq. 3 and 4 respectively, it is possible to obtain the weights W_{ICE} and W_m, thus completing the definition of W_{to} as from Eq. 2.

As a remark, it can be observed that accounting for the time-dependent variables σ_{ICE}^* and σ_m^* raises on one side the computational burden, but provides also a much greater flexibility in the design phase. To explain this point better, it may suffice to recall that a same power requirement can be met by means of an ICE and/or EM with high nominal power – with a high corresponding weight – and a low throttle setting, or conversely with less powerful energy conversion systems working close to full throttle. This way, the problem of understanding the best ratio between the nominal power of the ICE and EM, an issue typical to hybrid-electric aircraft, is expanded to include in the design solution the best way to manage the installed power over time and for different flight phases. Accounting for these variables at the design stage, the mission requirements, developed into simple equilibrium relations, allow to write the design problem in mathematical terms in a more comprehensive, well-posed form.

To manage this scenario more efficiently from a numerical standpoint, the design problem can be configured as an optimal problem, and made totally automatic. The adoption of an optimal approach allows to include a number of constraints at a limited cost, thus exploiting existing numerical techniques to obtain a design solution which is respective of as many requirements as possible since the earliest stage. The proposed resulting design technique will be thoroughly described in the next section.

4. Preliminary sizing through an optimal approach

An optimal approach can be adopted to automatically find a design point minimizing the design take-off weight W_{to}, subject to a set of constraints. The variables influencing most directly this quantity are the weight components summing up to W_{to} as from Eq. 2, which constitute a first set of optimization parameters – except W_{pl}, which is considered as an assigned constant from specifications. The most straightforward convex cost function associated to W_{to} is composed of the sum of its components squared, like

$$J = \left(\frac{W_{\text{ICE}}}{W_{\text{ICE,ref}}}\right)^2 + \left(\frac{W_f}{W_{f,\text{ref}}}\right)^2 + \left(\frac{W_m}{W_{m,\text{ref}}}\right)^2 + \left(\frac{W_{\text{bat}}}{W_{\text{bat,ref}}}\right)^2, \tag{27}$$

where subscript $(\cdot)_{\text{ref}}$ indicates a fixed normalization factor.

As noted above, the instantaneous value of required power is changing over time, hence making the throttle setting σ^*_{ICE} and σ^*_m functions of time. As explained at the end of the previous section, these functions can be considered as optimization parameters. Due to their value being limited between 0 and 1 by constitution, no further normalization is deemed necessary.

Therefore, the optimization problem leading to the design solution can be formally written as

$$\min_{\boldsymbol{q}} J \text{ s.t. } \boldsymbol{H}, \tag{28}$$

where parameters $\boldsymbol{q} = \{W_{\text{ICE}}, W_f, W_m, W_{\text{bat}}, W_e, \sigma^*_{\text{ICE}}, \sigma^*_m\}$, and $\boldsymbol{H}$ represents a set of constraints that will be analyzed in the following, showing how to profitably use the flight mechanics models introduced in the previous section.

It should be noted that the proposed merit function privileges the standpoint of the aircraft designer, targeting the take-off weight which is proportional to production cost [11, 27, 28] and is usually targeted to ensure coping with certification limits. While other choices of the merit function may privilege the operative cost of greater interest for operators by targeting fuel and electrical energy expenditure in flight, the adopted cost function has been deemed suitable for the scope of the paper, focused on an aircraft sizing technique.

4.1. Performance computation for constraint evaluation

The passages leading to the evaluation of the set of constraints $\boldsymbol{H}$ for every assigned value of the optimization parameters $\boldsymbol{q}$ will be described here step-by-step. Starting from the initialization of the computation, the following passages can be envisaged

- $P_{\mathrm{ICE},n}$ is computed from W_{ICE} through Eq. 3
- $P_{m,n}$ is computed from W_m through Eq. 4
- from an assigned value of the ratio W_{to}/S – which may be chosen based on a preliminary analysis of the SMP – and from that of W_{to} obtained from the current weights in the array of parameter $\boldsymbol{q}$, surface S is obtained
- starting values of time varying quantities are attributed as initial values for the take-off phase, i.e. the first phase in the flight profile

$$\begin{cases} W^{\mathrm{to}}(t_0^{\mathrm{to}}) = W_{\mathrm{to}} \\ W_f^{\mathrm{to}}(t_0^{\mathrm{to}}) = W_f \\ E_{\mathrm{bat}}^{\mathrm{to}}(t_0^{\mathrm{to}}) = \dfrac{W_{\mathrm{bat}} e_{\mathrm{bat}}}{g} \\ E_f^{\mathrm{to}}(t_0^{\mathrm{to}}) = \dfrac{W_f e_f}{g} \\ E_0^{\mathrm{to}}(t_0^{\mathrm{to}}) = E_{\mathrm{bat}}^{\mathrm{to}}(t_0^{\mathrm{to}}) + E_f^{\mathrm{to}}(t_0^{\mathrm{to}}) \end{cases} . \tag{29}$$

The superscript $(\cdot)^{\mathrm{to}}$ in Eq. 29 indicates a time-varying quantity in the take-off phase, and substitutes the generic function of time marked with $(\cdot)^*$ previously introduced.

Next, the performance corresponding to the current setting of the parameters $\boldsymbol{q}$ can be analyzed sequentially for each phase of the flight. The take-off phase can be managed as follows

- the value of V^{to} is computed from vertical equilibrium as $V^{\mathrm{to}} = \sqrt{\frac{2W^{\mathrm{to}}}{\rho^{\mathrm{to}} S C_L^{\mathrm{to}}}}$
- recharge power should be set to an assigned value, a possible choice being zero – $P_{\mathrm{rec}}^{\mathrm{to}} = 0$ – meaning that during take-off no power is used to recharge the batteries
- the energy battery flow $\dot{E}_{\mathrm{bat}}^{\mathrm{to}}$ is computed from Eq. 10
- the available power P_a^{to} is computed from Eq. 9
- the length of the take-off run L^{to} is computed integrating Eq. 8
- isolating $\dot{V}$ from Eq. 5 and substituting Eq. 6 and 7 in it, the take-off time can be computed as $T^{\mathrm{to}} = \int_0^{V^{\mathrm{to}}} \frac{\mathrm{d}V}{\dot{V}}$, as previously highlighted
- the fuel flow can be computed as $\dot{W}_f^{\mathrm{to}} = \frac{\sigma_{\mathrm{ICE}}^{\mathrm{to}} P_{\mathrm{ICE},n} g}{\eta_{\mathrm{ICE}} e_f}$
- fuel weight for take-off is computed as $W_f^{\mathrm{to}}\left(t_0^{\mathrm{to}} + T^{\mathrm{to}}\right) = W_f^{\mathrm{to}}\left(t_0^{\mathrm{to}}\right) - \dot{W}_f^{\mathrm{to}} T^{\mathrm{to}}$, and similarly $W^{\mathrm{to}}\left(t_0^{\mathrm{to}} + T^{\mathrm{to}}\right) = W^{\mathrm{to}}\left(t_0^{\mathrm{to}}\right) - \dot{W}_f^{\mathrm{to}} T^{\mathrm{to}}$

- the corresponding fuel energy for take-off can be computed as $E_f^{\mathrm{to}} = W_f^{\mathrm{to}} e_f$, whereas battery energy for take-off can be obtained as $E_{\mathrm{bat}}^{\mathrm{to}} = \dot{E}_{\mathrm{bat}}^{\mathrm{to}} T^{\mathrm{to}}$. The total stored energy needed for take-off is $E_0^{\mathrm{to}} = E_{\mathrm{bat}}^{\mathrm{to}} + E_f^{\mathrm{to}}$.

A synthetic flowchart of this process is presented in Fig. 4.

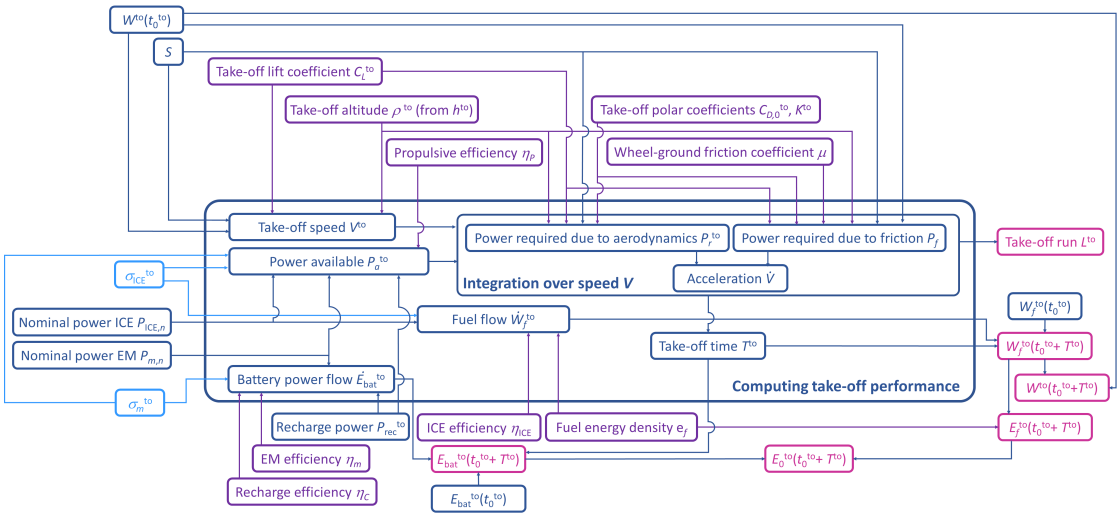

Figure 4: Flowchart of the take-off performance computation in the proposed optimal procedure. Dark blue: input from other processes. Light blue: optimization variables. Dark purple: assigned parameters. Light purple: output variables.

Three remarks apply to the presented procedure for the take-off phase. The first concerns the value to attribute to the recharge power $P_{\mathrm{rec}}^{\mathrm{to}}$. This value may be more generally treated putting it among the optimization parameters, yet setting this quantity to zero for take-off is a safer and more realistic assumption. Second, the values of the throttle parameters for both the ICE and EM groups shall not be considered as functions of time for take-off. This is reasonable considering the short duration of this particular flight phase, and also from a practical viewpoint, as a change in the throttle setting during take-off is not typical. Third, on account of the short duration of this phase, the computation of the change in fuel weight and of the corresponding energetic level is performed as shown, by hypothesizing a constant fuel flow computed *a posteriori*. This choice descends from considering weight as a constant in the equilibrium represented by Eq. 5, and the related Eq. 6 and 8. Again, this is made on account of the short extension in time of this phase.

The performance models for the next three phases of the mission, namely climb, cruise and loiter, include an integration forward in time, bearing results bound also to the assigned functions σ_{ICE}^* and σ_m^* in the array of parameters $\boldsymbol{q}$. For clarity, in practical terms these functions are defined over a time domain which is composed of four parts, corresponding to the four phases of the flight. For a generic time-evolving throttle

parameter σ^*, the time domain can be decomposed as follows

$$\sigma^* = \sigma(t) = \begin{cases} \sigma^{\text{to}}, t \in \left[0, T^{\text{to}}\right] \\ \sigma^{\text{climb}}, t \in \left[T^{\text{to}}, T^{\text{to}} + T^{\text{climb}}\right] \\ \sigma^{\text{cruise}}, t \in \left[T^{\text{to}} + T^{\text{climb}}, T^{\text{to}} + T^{\text{climb}} + T^{\text{cruise}}\right] \\ \sigma^{\text{loiter}}, t \in \left[T^{\text{to}} + T^{\text{climb}} + T^{\text{cruise}}, T^{\text{to}} + T^{\text{climb}} + T^{\text{cruise}} + T^{\text{loiter}}\right] \end{cases} \tag{30}$$

As highlighted above, take-off may be associated to constant values of the two throttle parameters, hence only two values are numerically assigned in this phase, one for the ICE and the other for the EM. For the other three phases both throttle parameters need to be assigned as functions of time.

The components of the computational procedure for climb, cruise and loiter are formally identical, hence they will be presented only once

- starting values of the functions of time W_f^*, W^*, E_{bat}^*, E_f^* and E_0^* are set to the level reached at the end of the previous phase of the flight
- the evolution of fuel weight W_f^* is obtained from the integral equation Eq. 14, and the fuel energy level E_f^* and overall weight W^* are similarly computed from Eq. 15 and 16
- power required P_r^* is computed from Eq. 13 as a function of time
- the time history of battery recharge power P_{rec}^* is obtained from Eq. 17
- the battery energy flow $\dot{E}_{\text{bat}}^*$ can be obtained as a function of time through Eq. 18, and the evolution of the energy level E_{bat}^* can be obtained correspondingly by integration as from Eq. 19
- total energy is obtained as a function of time from Eq. 20

Replicating this procedure for climb, cruise and loiter it is possible to obtain the values of the total fuel and battery energy from Eq. 23 and 24 for the mission.

A flowchart of the computation of climb performance, exemplifying also the procedure used for cruise and loiter, is presented in Fig. 5.

4.2. Analysis of the set of constraints

To better understand the need for a constraint set, it should be remarked at this point that, for the adopted optimization approach, a free choice of the parameters $\boldsymbol{q}$ does not guarantee meeting the required mission performance. Following an optimal approach aimed at finding a weight-optimal design point, the overall design weight is left free to change as a result of considering its components as optimization parameters, i.e. variables in the design problem. In order to obtain a design solution matching the mission requirements, the

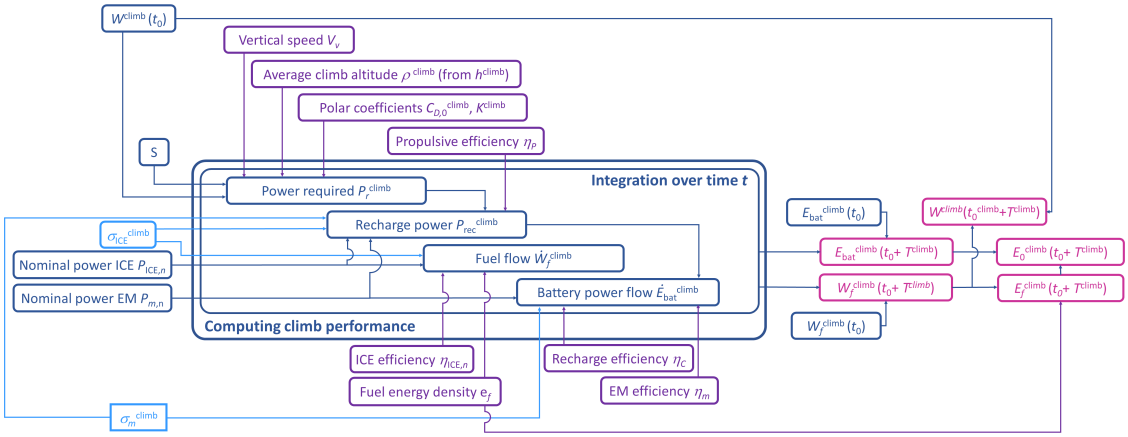

Figure 5: Flowchart of the climb performance in the proposed optimal procedure. Procedural structure valid also for cruise and loiter. Dark blue: input from other processes. Light blue: optimization variables. Dark purple: assigned parameters. Light purple: output variables.

performance obtained from the current value of the parameters needs to be compared to the desired values. It is clear that, with the adopted structure of the merit function, the optimum will always be dictated by the most requiring among the applied constraints – in other words, one or more constraints will be always active in the optimal condition. This fact is inherent to the considered structure of the problem and it is not an issue in itself, provided a suitable solution method is adopted. Care has been taken to design a set of constraints limiting the space of feasible solutions with a regular boundary, this way easing the stability of convergence of the optimizer to the actual optimum.

Before describing the set of constraints explicitly applied to the solution, it should be noted that meeting the requirements related to climb, cruise and loiter – i.e. vertical speed, range and endurance – is obtained implicitly by setting the time duration of these phases in the forward integration phase described previously, for assigned values of the speed. As a matter of fact the evolution in time of weight and energy quantities, which will be constrained with the following explicit requirements, is strictly bound to the extension of the time frames over which the performance models have been applied.

The set of optimization constraints $\boldsymbol{H}$ can be imposed based on quantities computed through the point-by-point procedure presented in this paragraph.

The first equation in the set binds the value of the empty weight W_e to that of W_{to}. As mentioned above, the uncertainties related to the parameters of the regression in Eq. 1, which is necessarily based on aircraft which are not representative of the target type – as no hybrid-electric aircraft has reached production at the time of writing – a formulation through two inequality constraints can be adopted, thus mathematically expressing the request of the solution to fall within a prescribed distance from the regression line on the plane $\log(W_{\text{to}})$ vs. $\log(W_e)$. Two relative distances β_{upper} and β_{lower} can be defined to express the maximum

acceptable drift of the design solution from the regression line, respectively by excess or defect. For the current value of parameter W_e in $\boldsymbol{q}$, from Eq. 1 it is possible to compute an upper value $W_{\text{to,upper}} = \beta_{\text{upper}} e^{A+B\log(W_e)}$, and similarly $W_{\text{to,lower}}$ with β_{lower} instead of β_{upper}. Then in analytic terms the corresponding inequality constraint can be expressed as

$$H_1 : W_{\text{to}} \in [W_{\text{to,lower}}, W_{\text{to,upper}}] . \tag{31}$$

As noted above, the reference surface S necessary for explicitly carrying out the computations of the performance is obtained from the current W_{to} and an assigned wing loading W_{to}/S. This quantity can be smartly chosen according to an analysis of the sizing matrix plot (SMP) [11, 24]. This plot is a representation of certification and performance requirements on the plane (W_{to}/P_n) vs. (W_{to}/S), where (W_{to}/P_n) represents the nominal power loading. An integrated design procedure where the choice of the design point on the SMP – i.e. in terms of a value for both (W_{to}/P_n) and (W_{to}/S) – is used to initialize the explicit solution of the design problem, based on mission profile requirements and a historical regression curve, can be envisaged for small purely electric aircraft [11]. For the corresponding hybrid-electric case the role of the SMP can be the same, and both design values of (W_{to}/P_n) and (W_{to}/S) can be specified before launching the optimization, based on a preliminary analysis of the plot and choosing a feasible design point with respect to the constraints reported on it. In case a sufficient margin has been left between the selected design point and the envelope of constraints on the SMP, differently from the purely electric case, the requirement on power loading can be imposed here through inequality constraints. In particular, if (W_{to}/P_n) is left free to change for an assigned W_{to} – i.e. its components in $\boldsymbol{q}$ –, then nominal power can be changed by the optimization algorithm, thus possibly finding a more optimal design solution. The admissible change in nominal power can be imposed through parameters θ_{upper} and θ_{lower}, such that $P_{n,\text{upper}} = \theta_{\text{upper}} P_n$ and $P_{n,\text{lower}} = \theta_{\text{lower}} P_n$. The corresponding inequality constraints apply to P_n, which for the hybrid-electric case is $P_n = P_{\text{ICE},n} + P_{m,n}$, so that

$$H_2 : P_n \in [P_{n,\text{lower}}, P_{n,\text{upper}}] . \tag{32}$$

It can be noted that the meaning of the upper and lower limits in Eq. 32 is different, as the former reflects the need to avoid excessive power for the mission, and the corresponding value may be imposed on the basis of cost constraints, whereas the lower stems from the need to satisfy performance or regulation constraints accounted for on the SMP.

Based on the approach selected to treat the take-off phase, it should be noted that the value of the runway length L^{to} is obtained as a result of the computation. This value can be constrained to make sure that the requirement usually formulated imposing an assigned $L^{\text{to}}_{\text{max}}$ is met, yielding

$$H_3 : L^{\text{to}} \leq L^{\text{to}}_{\text{max}}. \tag{33}$$

Concerning specifically the battery component, an inequality constraint shall be put on the power flow $\dot{E}^*_{\text{bat}}$, which should never exceed the value defined through the power density parameter typical to the adopted

battery technology, given a value of battery weight W_{bat}. In analytical terms,

$$H_4 : \max |\dot{E}^*_{\text{bat}}| \leq \frac{W_{\text{bat}} p_{\text{bat}}}{g}. \tag{34}$$

Similarly, the value of the energy stored in the battery cannot exceed the maximum capacity obtained through W_{bat} and e_{bat}, yet for inherent battery stability issues it can never descend below a minimum value expressed as a fraction $\nu \in (0, 1)$ of the maximum capacity, so that

$$\begin{aligned} H_5 : \max E^*_{\text{bat}} &\leq \frac{W_{\text{bat}} e_{\text{bat}}}{g} \\ H_6 : \min E^*_{\text{bat}} &\geq \nu \frac{W_{\text{bat}} e_{\text{bat}}}{g} \end{aligned}. \tag{35}$$

Considering the physics behind the power flowchart on which the energy model of the aircraft is based, the recharge power P^*_{rec} should not decrease below zero, meaning that the recharge power flow can be oriented from the ICE group towards the battery and not vice versa. In analytical terms this implies

$$H_7 : \min P^*_{\text{rec}} \geq 0. \tag{36}$$

The ICE in the proposed power-train supplies power to the batteries and to the propeller. Therefore, the battery recharge power needs to be a fraction of the total power produced by the ICE, thus avoiding the electric motor to recharge the batteries. For this reason, a corresponding constraint is put in the following terms

$$H_8 : \min (\sigma^*_{\text{ICE}} P_{\text{ICE,n}} - P^*_{\text{rec}}) \geq 0. \tag{37}$$

The evolution of fuel weight over time can be constrained so that the value of W^*_f would never descend below zero. Hence

$$H_9 : \min W^*_f \geq 0. \tag{38}$$

As the energy level of the hydrocarbon fuel can be obtained from the current fuel weight W^*_f by multiplication, constraint H_9 implicitly monitors also E^*_f.

Finally, as noted earlier in this work, on account of the fact that the flight profile is not strictly limited to the phases explicitly considered in the performance model – for instance, descent and landing are not considered –, a residual on the total stored energy can be imposed at the end of the flight performance computations. In practical terms, a minimum final total stored energy can be imposed applying a relative safety factor ξ_{lower} to the initial energy, such that $E^{\text{loiter}}_{0,\text{final}_{\text{min}}} = \xi_{\text{lower}} E^{\text{to}}_{0,\text{initial}}$. Similarly, to avoid an excessive weight penalty on account of a too high final energy residual, it is possible to introduce a factor ξ_{upper}, such that $E^{\text{loiter}}_{0,\text{final}_{\text{max}}} = \xi_{\text{upper}} E^{\text{to}}_{0,\text{initial}}$. By observing that the total stored energy can only decrease during the flight, it is possible to write the corresponding constraint as

$$H_{10} : E^{\text{loiter}}_{0,\text{final}} \in [E^{\text{loiter}}_{0,\text{final}_{\text{min}}}, E^{\text{loiter}}_{0,\text{final}_{\text{max}}}], \tag{39}$$

where subscripts $(\cdot)_{\text{initial}}$ and $(\cdot)_{\text{final}}$ indicate the evaluation of the corresponding quantity at the beginning and at the end of the considered flight phase.

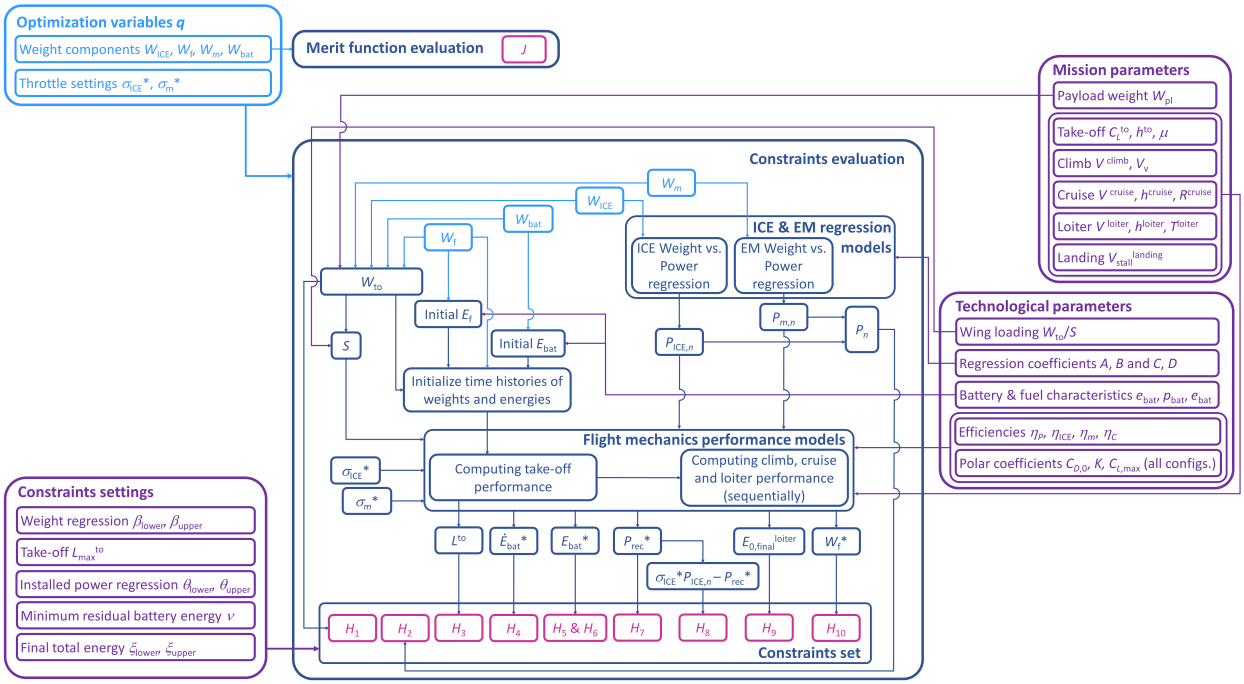

Figure 6: Flowchart of the optimal procedure. Dark blue: internal variables and processes. Light blue: optimization variables. Dark purple: assigned parameters. Light purple: output variables.

A schematic representation of the optimization procedure is presented in Fig. 6.

For easing the presentation, the set of constraints $\boldsymbol{H}$ has been described without reporting any normalization value. Clearly, in view of the different nature of the physical quantities treated in each expression of the $\boldsymbol{H}$ set, in the implementation stage these expressions may be normalized with respect to fixed reference values chosen arbitrarily, in order to ease the solution by means of an automated optimization algorithm.

5. Numerical results

5.1. Problem implementation

In order to treat the time-continuous functions σ_{ICE}^* and σ_m^* in the array of parameters $\boldsymbol{q}$ in a numerical procedure, it is necessary to introduce a discretization of the time domain, and a piece-wise linear shape for

the generic σ^* function can be specified as

$$\sigma^*(t_k) = \sum_k \bar{\sigma}_k f_k(t), \quad f_k(t) = \begin{cases} 0, t < t_{k-1} \cup t > t_{k+1} \\ \dfrac{t - t_{k-1}}{t_k - t_{k-1}}, t_{k-1} \leq t \leq t_k \\ \dfrac{t - t_k}{t_{k+1} - t_k}, t_k < t \leq t_{k+1} \end{cases}, \tag{40}$$

where the amplitudes $\bar{\sigma}_k$, defined in a number equal to the time nodes in the discretization grid for both σ^*_{ICE} and σ^*_m, become optimization variables. The number of time nodes can be different for each of the sub-components of the overall time domain defined in Eq. 30, on account of the respective durations. As previously remarked, the take-off phase is associated to single values of the throttle setting parameters, which are considered constant – i.e. the definition in Eq. 40 becomes trivial for the case of take-off. Accounting for the transcription on a discretized domain of the time functions σ^*_{ICE} and σ^*_m, it is possible to re-define the array of optimal parameters $\boldsymbol{q}$ for a numerical implementation of the optimal problem as

$$\bar{\boldsymbol{q}} = \left\{ W_{\mathrm{ICE}}, W_f, W_m, W_{\mathrm{bat}}, W_e, \boldsymbol{s}^{\mathrm{to}}, \boldsymbol{s}^{\mathrm{climb}}, \boldsymbol{s}^{\mathrm{cruise}}, \boldsymbol{s}^{\mathrm{loiter}} \right\}. \tag{41}$$

In Eq. 41 the array $\boldsymbol{s}^{\mathrm{to}}$ is defined as

$$\boldsymbol{s}^{\mathrm{to}} = \left\{ \bar{\sigma}_{\mathrm{ICE},1}, \bar{\sigma}_{m,1} \right\}, \tag{42}$$

whereas $\boldsymbol{s}^{\mathrm{climb}}$, $\boldsymbol{s}^{\mathrm{cruise}}$ and $\boldsymbol{s}^{\mathrm{loiter}}$ are based on the same generic definition, yielding

$$\boldsymbol{s} = \left\{ \bar{\sigma}_{\mathrm{ICE},1}, \bar{\sigma}_{\mathrm{ICE},2}, \ldots, \bar{\sigma}_{\mathrm{ICE},N}, \bar{\sigma}_{m,1}, \bar{\sigma}_{m,2}, \ldots, \bar{\sigma}_{m,N} \right\}, \tag{43}$$

where N indicates the number of allocation points in the part of the discretized time domain corresponding to the respective time function σ^*.

It should be remarked that the size of the set $\boldsymbol{q}$ may increase as a result of a finer discretization of the time domain. As the set of performance model does not include any high frequency dynamics, there is no danger of numerical divergence. Therefore, the choice of the discretization step is mainly bound to the desired precision in the solution over time, and in a preliminary analysis it is advisable to set it to a sufficiently wide value to save on the machine time for optimization.

5.2. Test case

As a test case for the proposed sizing procedure, the design of a motor-glider will be considered, similar to the cases presented in [11] and [22]. The key specifications and assumptions for the preliminary weight sizing will be quickly presented in the following, recalling data from previous works when pertinent.

5.2.1. Aircraft specifications

The coefficients for the weight regression in Eq. 1 are obtained based on a series of small electric aircraft having already flown or having reached the production stage. The corresponding parameters of the best fitting function are $A = 0.94$ and $B = 0.97$. Similarly, the coefficients in the relationship between nominal power and weight of the electric motor (Eq. 4) can be obtained from the data of the same group of aircraft and from some similar industrial specimens, yielding the values $C = 7.99{\cdot}10^{1}$ N and $D = 1.7{\cdot}10^{-3}$ s/m.

As anticipated, for the case of the ICE the relationship in Eq. 3 between weight and nominal power can be based on the regression of data from small marine engines. The same provider and product range considered in [22] have been considered [25], covering a power range between 1.8 and 14.7 kW, and a mass range between 18 and 55 kg.

Average energy and power densities of batteries can be prudentially estimated as $e_{\mathrm{bat}} = 136.5$ Wh/kg and $p_{\mathrm{bat}} = 761.9$ W/kg, taken from a previous study and made more conservative [11]. For hydrocarbon fuel, a value $e_f = 45$ MJ/kg can be assumed.

The efficiencies associated to the blocks in the flowchart in Fig. 3 have been set as shown in Table 1. The values of the propulsive efficiency η_P and of the nominal conversion efficiency of the ICE $\eta_{\mathrm{ICE,n}}$ have been assumed to typical values for the corresponding technologies for aeronautical use. The actual value of the ICE efficiency η_{ICE} is computed as a function of the power setting σ^*_{ICE}. The dependency of the ICE efficiency is often tabulated as a function of multiple parameters, typically rotational speed and power. Herein a simplified dependency was implemented, based on the hypothesis of a fixed operational trajectory on this plane, i.e. one power value for every rotor speed. The model was set in order to yield the nominal efficiency at nominal power, i.e. $\eta_{\mathrm{ICE,n}} = \eta_{\mathrm{ICE}}\,(\sigma_{\mathrm{ICE}} = 1)$. The efficiency decreases following a monotonic nonlinear function to around 12% of the nominal value for a $\sigma^*_{\mathrm{ICE}} = 0.6$, fitting experimental data from a lab ICE. Considering the electric part – η_m of the electric motor and η_C of the battery recharging process – as reliable measures for aeronautical components are not available in sufficient numbers, values typical to industrial components of comparable weight, power and energy have been considered. Thanks to the typically low scatter of these conversion efficiency values, this assumption should not be dramatically inaccurate.

η_P	0.80
$\eta_{\mathrm{ICE,n}}$	0.30
η_m	0.90
η_C	0.60

Table 1: Efficiency values for the key components of the propulsion system.

The flight profile considered for the mission is composed of four phases - take-off, climb, cruise and loiter. The corresponding key performance requirements are specified in Table 2.

$L^{\text{to}}_{\text{max}}$ [m]	200
h^{to} [m]	3000
μ [-]	0.030
V^{climb} [kn|m/s]	$1.2\text{V}^{\text{landing}}_{\text{stall}}$
V_v [ft/min|m/s]	400|2.02
h^{cruise} [m]	3000
V^{cruise} [kn|m/s]	90|46.3
R^{cruise} [km]	300
h^{loiter} [m]	3000
V^{loiter} [m/s]	$0.9\text{V}^{\text{cruise}}$
T^{loiter} [min]	15
$V^{\text{landing}}_{\text{stall}}$ [kn|m/s]	40|20.6

Table 2: Performance requirements for the considered mission profile.

Mission requirements are negotiated in order to assemble a profile which could be covered by a motor-glider built as a purely electric aircraft at the current level of technology. Applying the procedure presented in [11] it is possible to complete the preliminary sizing of a purely electric aircraft based on these requirements, which can be used as a reference to compare the outcome of the sizing of a hybrid-electric aircraft. As previously highlighted, a key passage in both sizing procedures – for the purely electric and hybrid-electric aircraft – is the choice of the design point in terms of wing loading $\frac{W_{\text{to}}}{S}$ and power loading $\frac{W_{\text{to}}}{P_n}$. The SMP for the proposed example is presented in Fig. 7. The curves on the SMP coming from the mission profile include take-off, cruise, loiter and landing performance, whereas those coming from FAR-23 standard, adopted as sizing guidelines considering the weight category and intended mission of the aircraft, are related to climb performance.

In order to produce the SMP it is necessary to assign the polar of the aircraft in take-off, landing and clean configurations. The corresponding coefficients of the usual parabolic model are presented in Table 3.

	Clean	Take–off	Landing
$C_{D,0}$	0.0110	0.0310	0.1010
$C_{L,\text{max}}$	1.5	1.5	2.2
K	0.0128	0.0128	0.0141

Table 3: Polar coefficients for different configurations.

A possible rule to choose the optimal design point on the SMP is that of simultaneously maximizing both $\frac{W_{\text{to}}}{P_n}$ and $\frac{W_{\text{to}}}{S}$. To explain that, for an assigned take-off weight W_{to} a higher power loading implies a lower

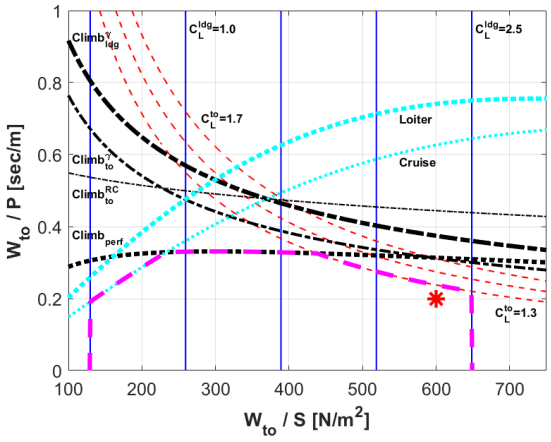

Figure 7: Sizing matrix plot for the considered design problem. Curves referring to both standard rules and mission requirements. Blue solid vertical lines: landing for various C_L. Red dashed lines: take-off run for various choices of C_L^{to}. Black dash-dotted lines: climb (two in take-off configuration with assigned climb angle γ and rate V_v, one in landing configuration with assigned angle γ as specified by FAR-23). Black dotted line: climb with assigned speed and rate V_v from mission profile. Cyan dotted lines: cruise and loiter. Magenta dashed line: envelope. Red star: reference design condition, adopted initialization values for optimization.

installed power, thus usually lowering engine – or motor – cost and size, whereas a higher wing loading would result in a shorter, more compact wing, which may help with handling qualities and aircraft storage issues. The choice of the design point at $\frac{W_{\text{to}}}{P_n} = 0.2$ s/m and $\frac{W_{\text{to}}}{S} = 600$ N/m^2 as shown in Fig. 7 follows these criteria, while accounting for a safety margin with respect to the constraints.

It should be remarked that the choice of the design values of $\frac{W_{\text{to}}}{P_n}$ and $\frac{W_{\text{to}}}{S}$ can be done following other processes different from the SMP, and as a matter of fact the optimization procedure for the hybrid-electric aircraft allows to account for a range of design values for the $\frac{W_{\text{to}}}{P_n}$ parameter. In this sense, the optimal design approach introduced herein for hybrid-electric aircraft allows to relax the need for an *a priori* choice of this design parameter, which on the contrary was typical to the procedures presented in [11] and [22]. As a consequence, the selection of a value for the ratio $\frac{W_{\text{to}}}{P_n}$ is basically that of a starting point for the optimization process, whereas $\frac{W_{\text{to}}}{S}$ will be kept fixed throughout the design process.

5.2.2. Requirements for optimal design

In order to practically implement the problem in Eq. 28 it is necessary to assign limit values for all constraining expressions in $\boldsymbol{H}$.

The tolerance factors β_{upper} and β_{lower}, allowing to relax the adherence of the design solution to the historical regression line in Eq. 1, can be specified to 1.05 and 0.95 respectively. It is clear that the lower the confidence in the historical regression on weights, the higher will be the distance between β_{upper} and

β_{lower}, thus the wider the range of acceptable solutions. It should be stressed that these parameters have a potentially relevant impact on the solution, and care should be taken to avoid abusing them, thus excessively widening the acceptable drift of the solution from the regression line in Fig. 1.

The range for total installed power P_n in Eq. 32 is defined through the quantities θ_{upper} and θ_{lower}, which can be set to 1.5 and 0.95 respectively. The lower constraint on power θ_{lower} may be defined based on the distance of the reference value for $\frac{W_{\text{to}}}{P_n}$ from the boundary on the SMP. On the other hand, the upper limit θ_{upper} may be defined according to constraints on the size or cost of the propulsion group. In this particular case θ_{lower} was selected according to the SMP on Fig. 7, whereas the upper value θ_{upper} has been limited to avoid the solution drifting too far away from the starting point, which is known to correspond to a feasible, reference purely-electric design.

The residual state of charge of the battery has been set at $\nu = 15\%$, as dictated by technological limits bound to battery stability.

The energy level at the end of the mission profile should be set in order to account for those parts of the flight not explicitly considered, and also to ensure a sound level of robustness of the design. The landing phase is associated to energy and power expenditures significantly below each other phase. In terms of power, standard rules examined when studying the SMP include climb after aborted landing. Therefore the most requiring power requirement in landing configuration has been implicitly accounted for by suitably choosing $\frac{W_{\text{to}}}{P_n}$ and the related limits in Eq. 32. Concerning energy, considering Eq. 39 a final level of total energy between $\xi_{\text{lower}} = 5\%$ and $\xi_{\text{upper}} = 10\%$ of the initial value should be sufficient to cover landing, emergency maneuvers in approach and for assuring a certain level of robustness of the design with respect to changes to the mission profile as well as inaccuracies in the power and energy density estimates, without imposing an excessive toll on weight.

Besides the constraints in $\boldsymbol{H}$, it is possible to set some bounds to the quantities in $\bar{\boldsymbol{q}}$. All variables in $\bar{\boldsymbol{q}}$ are positive, and all components of arrays $\boldsymbol{s}^{\text{take-off}}$, $\boldsymbol{s}^{\text{climb}}$, $\boldsymbol{s}^{\text{cruise}}$, and $\boldsymbol{s}^{\text{loiter}}$ should not exceed 1. In order to further constrain the solution avoiding wasting time on unacceptably high values of weight, reasonable bounds may be put on all five weights appearing as parameters in Eq. 41, which obviously should not decrease below zero.

Thanks to its good regularity the optimal problem Eq. 28 can be solved numerically by deploying a standard optimization algorithm. Experiments have been carried out with both a genetic and a gradient-based algorithm in `Matlab`® environment. The latter is typically superior in convergence speed, and thanks to the regularity of the specific problem it can be safely selected as a standard way to practically manage the optimization procedure. In a preliminary validation stage the selected interior point algorithm has been tested with five different initial conditions, highlighting the robustness of the code with respect to this parameter.

The number of collocation points in the time grid and their density in the three flight phases of climb, cruise

and loiter has been investigated thoroughly. For the specific design problem presented here a number of 10 nodes for both climb and loiter and a number of 15 for cruise appear to represent a threshold for convergence of the solution. In other words, no significant alteration of the solution is obtained by further refining the discretization of the time domain, which would come at the price of a greater number of optimization variables and machine time.

5.2.3. Baseline hybrid-electric solution

The basic characteristics of the solution of the optimal design problem with the parameters specified in the previous paragraphs are presented in Table 4. It should be recalled that the optimal parameters in the table are only the values of the weight components W_{ICE}, W_f, W_m, W_{bat} and W_e, whereas the values of other quantities are obtained as functions of such quantities.

	Hybrid-electric	All-electric
W_{to}/g [kg]	585	856
W_{ICE}/g [kg]	65.3	0
W_f/g [kg]	42.6	0
W_m/g [kg]	10.7	17.2
W_{bat}/g [kg]	38.2	279
W_e/g [kg]	278.6	409
$P_{\text{ICE},n}$ [kW]	25.0	0
$P_{m,n}$ [kW]	14.8	52.5
S [m^2]	9.6	14.0

Table 4: Results of optimal hybrid-electric design under reference requirements. Comparison with respect to an all-electric design with similar requirements.

For a comparison, the corresponding weights of the all-electric design obtained as a result of the dedicated procedure introduced in [11] are shown on the rightmost column of the table.

In Fig. 8 are presented the optimal values of the throttle percentages for both the ICE and EM. As explained, the nodal values of these functions are optimization parameters too.

By inspecting the results for the hybrid-electric case on Tab. 4, it is possible to notice that the overall weight W_{to} is significantly lowered with respect to the purely electric case. Similarly, the value of W_e has been decreased visibly. It can be reported that the most stringent constraints on the optimal solution are the minimum value of fuel weight over time, set to be positive through H_9 in Eq. 38, the top battery energy value $\max E^*_{\text{bat}}$ from H_5 in Eq. 35 and the top value on W_{to} from H_1 in Eq. 31. This is in accordance with the expected tendency of the optimizer to reduce weight by loading the minimum energy possible, thus resulting

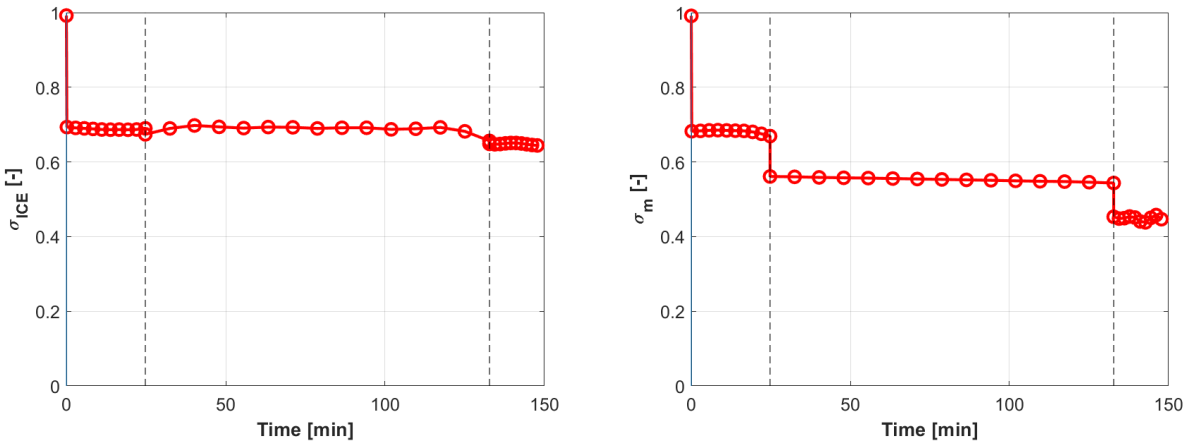

(a) (b)

Figure 8: Optimal time histories of σ_{ICE} (left) and σ_m (right) in reference design conditions. Circles: values corresponding to computation nodes in the time grid. Vertical dashed bars: initial times of cruise and loiter.

in minimum fuel weight at the end of the profile, and loading the batteries to their maximum capacity. Also the flexibility on the regression line in Eq. 1, represented by Eq. 31, is exploited to get an optimal condition where the difference between W_{to} and its component W_e is pushed towards the maximum attainable value.

The weights of the batteries and of the electric motor are lowered with respect to the purely electric design, but the overall nominal installed power, given by the sum of the nominal power figures $P_{\mathrm{ICE},n}$ and $P_{m,n}$, decreases to a less extent. Considering the significant reduction of W_{to}, this corresponds to a significant decrease of $\frac{W_{\mathrm{to}}}{P_n}$, which has been left free to change in a range as a result of constraint H_2 in Eq. 32. This decrease can be explained with a more thorough analysis of the take-off phase added in the present work, which bears possibly more stringent power requirements than for the previous all-electric case, and also with the strongly lower conversion efficiency of the ICE with respect to the EM, where both are now involved in the production of an available power output such to guarantee equilibrium.

The value of the wing reference surface S is visibly reduced, as a result of the fixed $\frac{W_{\mathrm{to}}}{S}$ and lowered W_{to}. The reduction in both W_{to} and S suggests a hybrid-electric solution which is generally more compact and lighter with respect to a purely electric design.

From Fig. 8 it is possible to notice that the optimal use of the installed power for the design mission is basically represented by an ICE working at maximum power during take-off – leftmost point on the plot – and at a continuous power between 60-70% throttle in the other phases. The EM should contribute with its maximum power during take-off, and to a significant extent between 40-70% throttle also during the other phases.

It is noteworthy that the change in weight is limited considering each phase of the flight, as can be seen

in Fig. 8 observing the very low adjustment of the throttle settings over a single phase necessary to satisfy equilibrium. This is due to the fact that the only weight which is evolving in time is that of fuel, which is a reduced fraction of the total. While this may suggest that a less accurate flight mechanics model may be employed with similar results, this cannot be a general conclusion, but limited to presented case and due to the very favorable polar and very low weight of the considered motor-glider. It can also be observed that the change in weight due to fuel burn is compensated in cruise by a decrease in the EM throttle setting. This may be due to the efficiency of the ICE depending on the ICE throttle, thus making a decrease in the latter more disadvantageous.

The time histories of the recharge power P_{rec}, the actual – i.e. not nominal – power available from the ICE and EM, $\sigma_{\text{ICE}} P_{\text{ICE},n}$ and $\sigma_m P_{m,n}$ respectively, and the required power $\frac{P_r^*}{\eta_P}$ are presented on the left plot in Fig. 9. To the right of the same figure are shown the energy levels corresponding to the battery, fuel and their total. It is possible to note that the battery energy level is decreasing sharply during climb, corresponding to a low recharging power. During cruise and loiter, the power produced by the EM is basically compensating for the propulsive power, whereas the ICE is used to slowly recharging the batteries, implying that the battery is slowly recharged at a constant rate, as can be seen on the right plot in Fig. 9. The battery energy level does never descend below a minimum as imposed through constraint H_6, where the final value of total energy is within the range prescribed through constraint H_{10}.

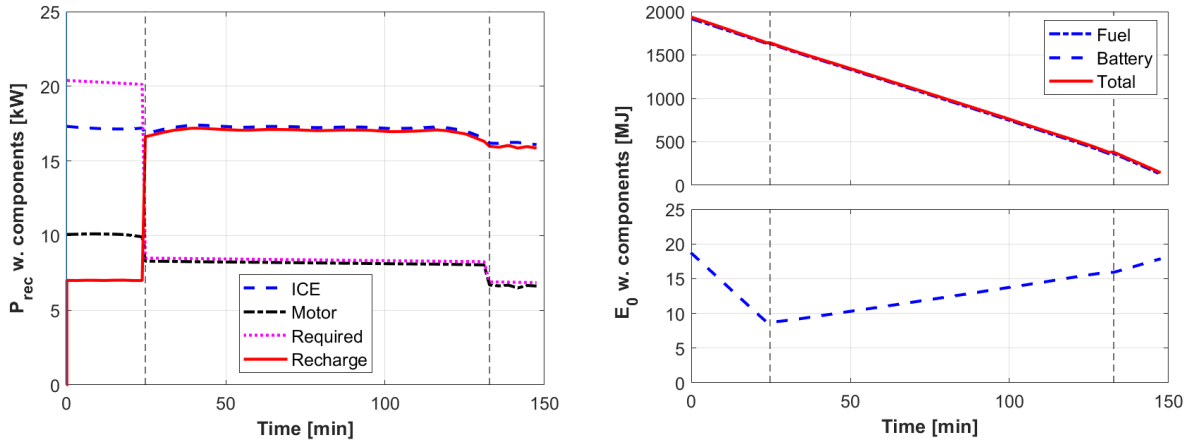

(a) (b)

Figure 9: Optimal time histories of recharge power and its components (left) and of total energy and its components (right). Vertical dashed bars: initial times of cruise and loiter. Left plot. Blue dashed: ICE. Black dash-dotted: EM. Purple dotted: required. Red solid: recharge. Right plot. Blue dash-dotted: fuel. Blue dashed: battery. Red solid: total.

From the description above, it can be highlighted that an optimal management of the installed power-train can turn out rather sophisticated, even considering a simplified mission profile as in this work. This stands in

support of the adoption of a comprehensive approach to the solution of the design problem, supported by an automated optimization algorithm, instead of a more traditional single-point trial and error search. In other words, the need to install a mix of electrical and internal combustion power typical to hybrid-electric aircraft broadens the space of design solutions. In this scenario, choosing the correct electric/hydrocarbon power mix for an assigned reference mission profile, without accounting for the actual time histories of output power, may lead to sub-optimal solutions, as shown by the fact that the two throttle settings – and especially σ_m as highlighted – change significantly over time in an optimal condition. Hence it makes sense to consider the values of both the installed power of the electric and internal combustion parts – through the corresponding weights in Eq. 2 and 27 – and the throttle parameters together in the set of design variables. Clearly, considering a more populated set of design parameters increases the size of the problem, and an optimal approach can be useful to manage this scenario more easily.

5.3. Sensitivity studies

After looking at the result of an optimal solution coping with all requirements, in a preliminary design it is usually recommendable to check how the solution would change for altered values of the requirements and properties of the aircraft. In this paragraph a few examples of parametric analyses will be shown, changing in a first stage the requirements on rate of climb, loiter time, and secondarily the specific energy and power of the batteries, the wing loading and the tolerance on the coefficients of the W_{to} vs. W_e regression. For each changed condition the optimization is performed finding the corresponding optimal design solution.

5.3.1. Rate of climb and loiter time

Figure 10 shows the result of a change on the requirement on the vertical speed V_v during climb and flight time T^{loiter} in loiter. It can be observed that generally speaking except for an increase for the top considered loiter time, the overall and empty weight components are largely unchanged. For lower loiter times the battery weight tends to be increased with respect to fuel weight (right plot). There is also a slight increase in the weight of the EM with an increase in both parameters.

Concerning the rate of climb, the strategies used to regulate power are shown for the two extreme considered cases of 400 ft/min (reference) and 700 ft/min in Fig. 11. The throttle setting for the ICE and EM is mostly upscaled in climb when passing from a lower to a higher V_v requirement, on account of the similar power $P_{\text{ICE},n}$ and $P_{m,n}$ (due to similar weight W_{ICE} and W_m), where the throttle settings in cruise and loiter are mostly unchanged.

Figures 10 left and 11 suggest that the optimal design solution to cope with a change in the climb requirements implies a more substantial change in the throttle settings than in weights. For a change in loiter time specifications, the throttle settings (not shown) are largely unchanged with respect to the reference, and the weights of the ICE, EM and corresponding energy storage systems are more visibly changed.

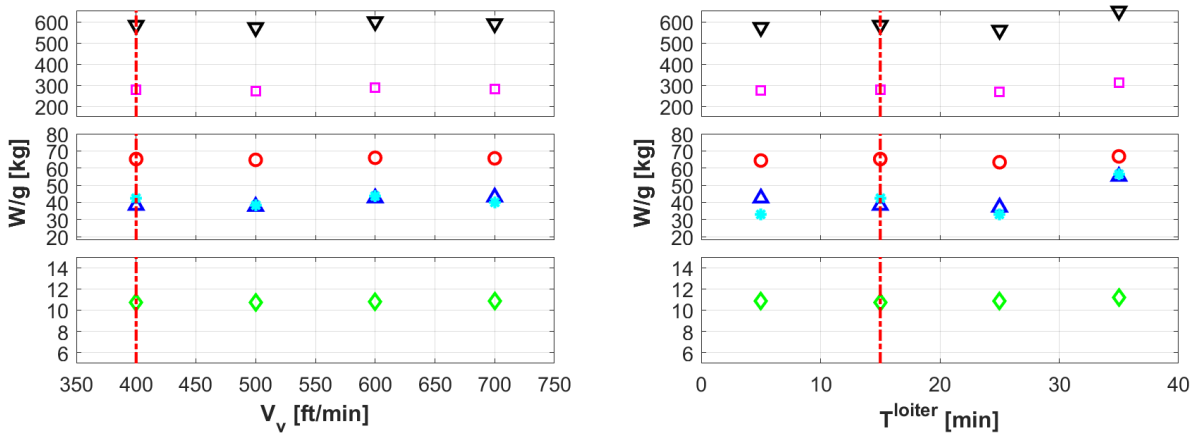

(a) (b)

Figure 10: Effect of the requirement on V_v (left) and T^{loiter} (right). Black triangles: take-off weight. Purple squares: empty weight. Red circles: ICE weight. Blue triangle: battery weight. Cyan stars: fuel weight. Green diamonds: EM weight. Red vertical bar: baseline solution.

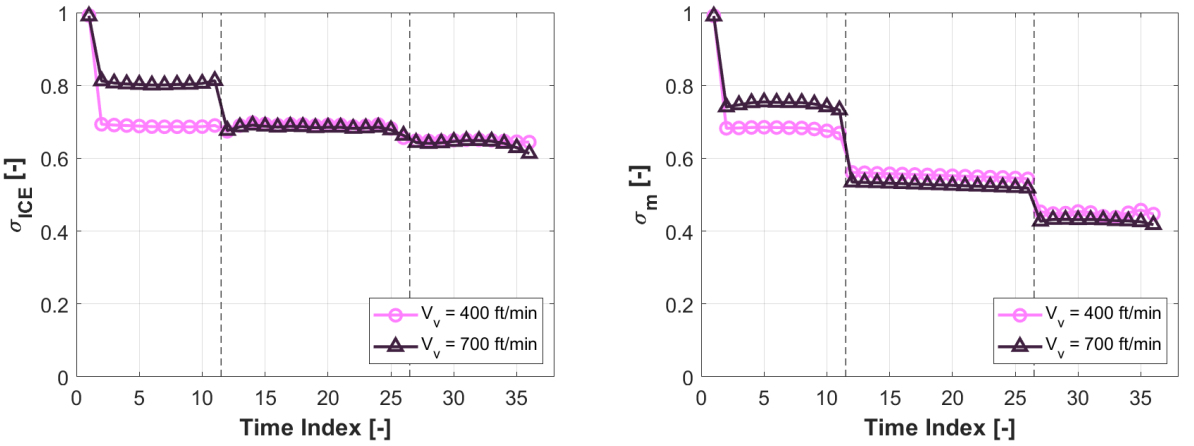

(a) (b)

Figure 11: Optimal time histories of σ_{ICE} and σ_m for the extreme considered values of V_v. Lighter line and circles: reference V_v. Darker line and triangles: top considered V_v. The markers correspond to computation nodes in the time grid. Vertical dashed bars: boundaries between flight phases.

5.3.2. Specific energy and power of batteries

The analysis concerning the effect of the battery specific energy and power has been carried out considering a simultaneous change of both e_{bat} and p_{bat} in order not to change their ratio with respect to the reference, thus better accounting for the technological features of these components. From Fig. 12 it is possible to notice the effect of the battery specifications is felt mainly on the battery and fuel weights, which tend to mutually compensate. When very low batteries specifications, actually below the current technological level, are considered (moving left on the plot), then the solution starts drifting towards a classic hydro-carbon fueled machine. This corresponds also to a lower overall weight as increasingly inefficient batteries are progressively eliminated. This effect highlights the necessity to use high-performing batteries to make a hybrid-electric solution convenient.

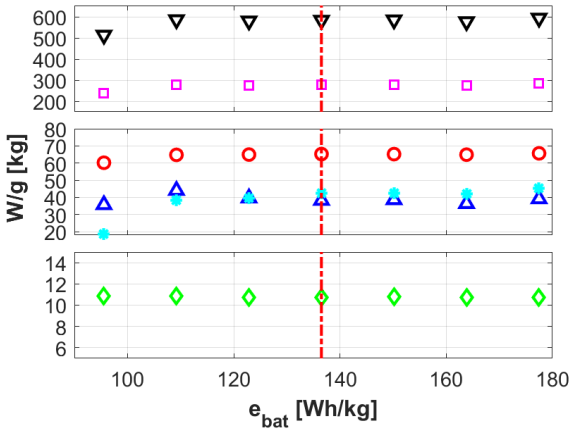

Figure 12: Effect of the requirement on e_{bat} and p_{bat}. Black triangles: take-off weight. Purple squares: empty weight. Red circles: ICE weight. Blue triangle: battery weight. Cyan stars: fuel weight. Green diamonds: EM weight. Red vertical bar: baseline solution.

The throttle settings (not shown) do not change in the overall shape from the reference solution, and the corresponding values change of 12% at most between extreme cases in climb.

5.3.3. Coefficients of W_{to} vs. W_e regression

Figure 13 shows the effect on the weights of optimal solutions obtained widening the interval $[\beta_{\text{lower}}, \beta_{\text{upper}}]$ symmetrically. The result has been plotted as a function of the half interval $\frac{1}{2}(\beta_{\text{upper}} - \beta_{\text{lower}})$.

From Fig. 13 it can be noticed that as the interval increases from zero the solution tends to be generally less heavy in terms of empty weight W_e, showing that a boundary zone around the regression line is exploited by the optimizer to decrease the value of the weight, pulling it down as much as allowed by the constraint H_1. The effect of this constraint is felt on the majority of the conditions analyzed in this work, and while this may be not general, it should be highlighted that the confidence interval $[\beta_{\text{lower}}, \beta_{\text{upper}}]$ may be set to

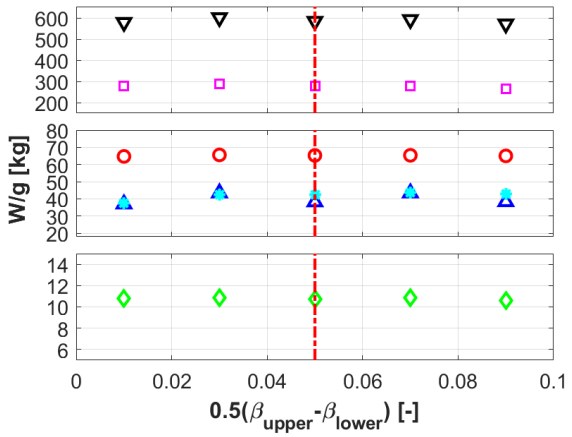

Figure 13: Effect of the characteristic values of β_{lower} and β_{upper} on the weight components. Black triangles: take-off weight. Purple squares: empty weight. Red circles: ICE weight. Blue triangle: battery weight. Cyan stars: fuel weight. Green diamonds: EM weight. Red vertical bar: baseline solution.

explore a wider space of solutions when the coefficients in Eq. 1 are not precisely known, or when their very values are under investigation.

5.3.4. Wing loading

Figure 14 presents the evolution of the optimal weight components for different $\frac{W_{\text{to}}}{S}$. The decrease in ICE and EM weight – and hence power – for lower values of the wing loading is justified for a motor-glider and the corresponding polar, recalling from vertical equilibrium that the inverse of lift-to-drag ratio is bound to a parasite drag component which is inversely proportional to $\frac{W_{\text{to}}}{S}$ and an induced component which is proportional to it. The former is very low for streamlined designs like the considered motor-glider, hence the latter dominates and pushes the lift-to-drag ratio higher for decreasing values of $\frac{W_{\text{to}}}{S}$. This implies a reduced power required for a lower $\frac{W_{\text{to}}}{S}$.

The behavior of the optimal solution for a lower $\frac{W_{\text{to}}}{S}$ suggests that the electric component is more advantageous or the solution is less sensitive to it due to the generally lower weight of the EM compared to the ICE, and as a result the design tends to feature a lower ICE weight, with a similarly powerful EM, and also a lower battery weight in accordance with a lower overall weight of the aircraft. The results in terms of σ_{ICE} (not shown for brevity) indicate that its value is generally higher for lower $\frac{W_{\text{to}}}{S}$ and smaller ICE, with an increase of the throttle up to 16% with respect to the baseline. This can be justified also by the increase in efficiency associated to a higher throttle setting for the ICE. The setting σ_m generally decreases for lower $\frac{W_{\text{to}}}{S}$ but to a lesser extent.

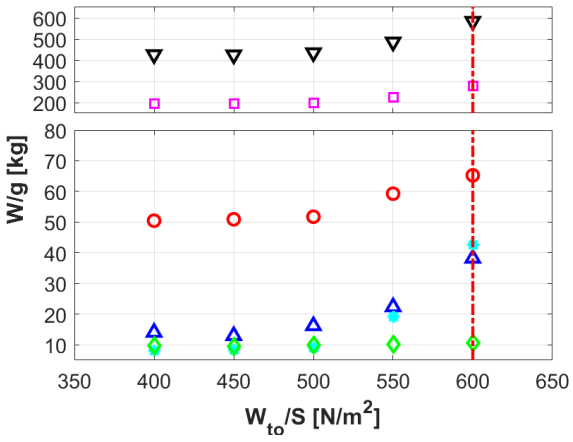

Figure 14: Effect of $\frac{W_{\text{to}}}{S}$. Black triangles: take-off weight. Purple squares: empty weight. Red circles: ICE weight. Blue triangle: battery weight. Cyan stars: fuel weight. Green diamonds: EM weight. Red vertical bar: baseline solution.

6. Conclusions

The present paper deals with a technique for the preliminary weight sizing of a hybrid-electric aircraft, with a primary application to light aviation. Due to the lack of a direct link between the features of the mission profile and all weight components contributing to the take-off weight, for hybrid-electric aircraft it is hard to apply well proven techniques generally adopted for conventionally powered aircraft, based on fuel fractions. Furthermore, the coexistence on the same aircraft of two radically different power-plants, i.e. internal combustion engines and electric motors, and of the corresponding energy storage systems, i.e. hydrocarbon fuel and batteries, makes the sizing process potentially complicated even in face of a rather simple mission profile.

In order to effectively tackle the sizing problem for hybrid-electric aircraft, a methodology is presented based on simple flight mechanics models, capable of translating requirements on performance indices characterizing the mission profile into power and energy requests. A general power flowchart of a possible hybrid-electric power-train is hypothesized for the task. The power and energy output requirements are linked to the weights of key components of the aircraft by means of statistical relationships based on real data.

The exact solution of equilibrium in the various phases of the flight, taking into account the different flight mechanics characteristics of each of them and the time-evolving weight of the aircraft, is guaranteed by scaling the nominal power of the fuel-burning engine and of the electric motor. Such throttle variables for the ICE and EM are interesting to study for a hybrid-electric aircraft, for they provide a significant insight into how to manage the installed power mix. From a design standpoint, they are considered as design parameters to be computed, similarly to the weight components contributing to take-off weight.

The solution algorithm adopted for the design problem considers the key weight components as inde-

pendent variables, together with the throttle parameters responsible for scaling the nominal power of the internal combustion engine and electric motor over time. An optimal approach is envisaged to solve the design problem, where the overall weight is minimized by demanding the selection of all weight components and the throttle settings of the propulsion system in time to an automated algorithm, while all conditions on the mission profile and equilibrium are applied as constraints. The choice of the overall weight as a target for the optimization may be supported also from the viewpoint of economics, as production cost is typically lower for smaller and lighter aircraft in the considered category. For the case of throttle variables, which are studied as functions of time, a collocation on a discretized time domain has been applied to allow a numerical implementation of the sizing procedure. The proposed set of constraints produces a well-posed mathematical problem. Thanks to the good regularity of the merit function and of the constraining equations, a robust solution can be obtained recurring to a standard gradient-based approach, making the outlined procedure especially useful in the negotiation of the requirements, when their respective effects on the outcome of the design is studied.

The proposed methodology has been tested designing at first a baseline hybrid-electric aircraft, corresponding to requirements which can be met with a fully-electric solution studied in other works, this way showing the predictable advantage in terms of weight that can be obtained by implementing a hybrid-electric solution. An extensive sensitivity analysis has been subsequently included and thoroughly commented. Both key mission specifications and technological characteristics have been selected as parameters, thus allowing to investigate their respective effects on the considered test case of a light motor-glider, showing technically relevant trends for the specific field of application. Furthermore, the good regularity of the design solutions with respect to changing parameters tends to support the potential of the proposed automatic design methodology as a robust tool to run reliable and time-effective analyses which are a typical necessity of the preliminary design stage.

The present paper makes use of some technological assumptions, some of which may be seen as a potential limitation of the scope of the results. In particular, the adopted regressions concerning power and weight of the internal combustion engine and electric motor are mainly based on a limited amount of data, and for the former these are not taken from the aeronautical field. Furthermore, the characterization of the power-train is simplified and not general. Nonetheless, this does not influence the suitability of the proposed procedure for the intended automated design task. Furthermore, care has been taken both to select data which are at least not incompatible with an aeronautical solution and to avoid futuristic assumptions concerning the mechanical or electrical properties of the subsystems, thus obtaining meaningful numerical results in the considered example. The level of detail chosen for modeling the power-train is compatible with the preliminary weight sizing phase of interest here. Clearly, more accurate results, especially of interest in a more advanced phase of the design, may be obtained for other specific applications when more accurate data are available,

and the design procedure may be also easily amended to cope with a higher number of components in the power-train, thus making the design solution more tailored to the problem at hand. In a similar potential design scenario, featuring a wider solution space than that considered in this work, the optimal approach presented herein would be even more valuable to allow obtaining a quick solution of the design problem, facilitating the preliminary design phase of a hybrid-electric aircraft modeled with a higher level of detail.

Acknowledgements

The contribution of professor Lorenzo Trainelli of the Department of Aerospace Science and Technology, Politecnico di Milano, in the discussion and revision of this paper is gretefully acknowledged.

Declaration of conflicting interests

The Author declares that there is no conflict of interest.

Funding

This research received no specific grant from any funding agency in the public, commercial, or not-for-profit sectors.

References

[1] C.A. Hall, and D. Crichton, Engine and Installation Configurations for a Silent Aircraft, ISABE, 1164(2005) 1-12.

[2] R. Kawai, Quiet Cruise Efficient Short Take-Off and Landing Subsonic Transport System, Technical Report NASA/CR2008-215141, NASA Glenn Research Center, Cleveland, OH, 2008.

[3] D. Miljkovic, J. Ivoevic, and T. Bucak, Psycho-Acoustical Ergonomics in a Light Aircraft Interior, in: 5th International Ergonomics Conference, Zadar, Croatia, June 12-15, 2013.

[4] P. Morrell, and C. Lu, Aircraft Noise Social Cost and Charge Mechanisms - A Case Study of Amsterdam Airport Schiphol, Transportation Research Part D, 5(2000) pp. 305-320.

[5] J.P. Cohen, and C.C. Coughlin, Spatial Hedonic Models of Airport Noise; Proximity and Housing Prices, Journal of Regional Science, 48(2008) 859-878.

[6] K. Ozawa, Lithium Ion Rechargeable Batteries, Wiley-VCH, First Edition, 2009.

[7] L.W. Traub, Range and Endurance Estimates for Battery-Powered Aircraft, Journal of Aircraft, 48(2011) 703-707.

[8] W. Cao, B.C. Mecrow, G.J. Atkinson, J.W. Bennett, and D.J. Atkinson, Overview of Electric Motor Technologies Used forMore Electric Aircraft (MEA), IEEE Transaction on Industrial Electronics, 59(2012) 3523–3531.

[9] M. Hagen, S. Dörfler, P. Fanz, T. Berger, R. Speck, J. Tübke, H. Althues, M.J. Hoffmann, C. Scherr, and S. Kaskel, Development and Costs Calculation of Lithium-Sulfur Cells with High Sulfur Load and Binder Free Electrodes, Journal of Power Sources, 224(2013) 260-268.

[10] M. Hagen, D. Hanselmann, K. Ahlbrecht, R. Maa, D. Gerber, and J. Tbke, Lithium-Sulfur Cells: The Gap between the State-of-the-Art and the Requirements for High Energy Battery Cells, Advanced Energy Materials, 5(2015).

[11] C.E.D. Riboldi, and F. Gualdoni, An Integrated Approach to the Preliminary Weight Sizing of Small Electric Aircraft, Aerospace Science and Technology, 58(2016) 134-149.

[12] A. Broglia, L. Clozza, M. Russo, C. Spada, L. Vendemini, A.G. Zuanetti, C.E.D. Riboldi, and L. Trainelli, FLYNK - The Future All-Electric Commuter Concept for Metropolitan Areas, in: Italian Association of Aeronautics and Astronautics (AIDAA) 24th International Conference, Palermo-Enna, Italy, September 18-22, 2017.

[13] M.A. Kromer, and J.B. Heywood, Electric Powertrains: Opportunities and Challenges in the U.S. Light–Duty Vehicle Fleet, Technical Report LFEE2007-03RP, Sloan Automotive Laboratory, Massachusetts Institute of Technology, Cambridge, MA, 2007.

[14] G. Pistoia, Electric and Hybrid Vehicles, Elsevier, First Edition, 2010.

[15] T. Choi, D. Soban, and D. Mavris, Creation of a Design Framework for All-Electric Aircraft Propulsion Architectures, 3rd International Energy Conversion Engineering Conference, San Francisco, CA, August 15-18, 2005.

[16] C. Pornet, C. Gologan, P.C. Vratny, A. Seitz, O. Schmitz, A.T. Isikveren, and M. Hornung, Methodology for Sizing and Performance Assessment of Hybrid Energy Aircraft, Journal of Aircraft, 52(2014) 341-352.

[17] C. Pornet, and A.T. Isikveren, Conceptual Design of Hybrid–Electric Transport Aircraft, Progress in Aerospace Sciences, 79(2015) 114-135.

[18] Y. Fefermann, C. Maury, C. Level, K. Zarati, J.P. Salanne, C. Pornet, and A.T. Isikveren, Hybrid-Electric Motive Power Systems for Commuter Transport Applications, in: Proceedings of the 30th Congress of the International Council of the Aeronautical Sciences, Daejeon, South Korea, September 25-30, 2016.

[19] C. Friedrich, and P.A. Robertson, Hybrid-Electric Propulsion for Aircraft, Journal of Aircraft, 52(2015) 176-189.

[20] G.E. Bona, M. Bucari, A. Castagnoli, and L. Trainelli, Flybrid: Envisaging the Future Hybrid-Powered Regional Aviation, in: AIAA/3AF Aircraft Noise and Emissions Reduction Symposium, Atlanta, GA, June 16-20, 2014.

[21] A. Bernasconi, F. Biondani, L. Capoferri, A. Favier, C. Velarde Lopez de Ayala, C.E.D. Riboldi, L. Trainelli, Conceptual Design of a Structural-Battery Hybrid-Electric Aircraft, in: Italian Association of Aeronautics and Astronautics (AIDAA) 24th International Conference, Palermo-Enna, Italy, September 18-22, 2017.

[22] C.E.D. Riboldi, F. Gualdoni, and L. Trainelli, Preliminary Weight Sizing of Light Pure–Electric and Hybrid–Electric Aircraft, Transportation Research Procedia, 29(2018) 376-389.

[23] J. Roskam, Airplane Design, Part I–VII, DARcorporation, Second Edition, 2003.

[24] D.P. Raymer, Aircraft Design: A Conceptual Approach, AIAA Education Series, Fifth Edition, 2012.

[25] Yamaha Motor Corporation, Boat Motor; Portable Outboard, yamahaoutboards.com, 2017.

[26] J.D. Anderson Jr., Introduction to Flight, McGraw-Hill International Edition, Eighth Edition, 2016.

[27] S. Gudmundsson, General Aviation Aircraft Design, Butterworth–Heinemann, First Edition, 2013.

[28] E.A. Estrada Rodas, J.H. Lewe, and D. Mavris, Feasibility Focused Design of Electric On–Demand Aircraft Concepts, in: 14th AIAA Aviation Technology, Integration, and Operations Conference, Atlanta, GA, June 16–20, 2014.